2nd January 2026

Structural & tectonic setting of pegmatite dykes in the Damara Orogen, Namibia

Thomas Lloyd Jones

Email: thomas.jones@tljgeo.com

This work formed part of T. Jones' PhD research at the University of the Witwatersrand. It has not been examined and is instead made publicly available for industry and academic use.

-

Jones, T.L. 2026. Structural & tectonic setting of pegmatite dykes in the Damara Orogen, Namibia. *Unpublished PhD research report, University of the Witwatersrand, South Africa*.

Research Sponsors:

Deep Yellow LIMITED

TLJ Structural Geology Consulting Ltd

SOCIETY OF ECONOMIC GEOLOGISTS FOUNDED 1920

cimera DSTI-NRF Centre of Excellence for Integrated Mineral and Energy Resource Analysis

Economic Relevance

This study presents a detailed structural and tectonic analysis of uranium-bearing pegmatite and leucogranite dykes in the southern Central Zone of the Damara Orogen, Namibia — one of the world's key uranium provinces. The work integrates comprehensive field mapping, structural measurements, and conceptual modelling to explain how pegmatite dykes are oriented, deformed, and distributed around dome structures in the mid-crust of the Damara Belt. The findings provide a direct link between deformation processes and exploration targeting, enabling structural data to be translated into an understanding of mineralised dyke geometry.

Keywords:
Leucogranite, pegmatite, orogen, mineralisation, uranium, folding.

Highlights:

I. Pegmatite dykes are intensely folded in a constrictional regime
II. Simple field-based structural framework guides future mineral exploration
III. Regional tectonic setting involved lateral constrictional flow of the mid-crust
IV. A single phase of progressive deformation explains the regional structural evolution

Key structural relationships relevant to exploration:

Dataset / Feature	Relationship to other structures	Exploration / modelling use	Importance
 **Lineations (L-tectonites, rodding, mullions)**	Consistently parallel to fold axes and dyke strike	Key predictor of dyke trend	Very high
 **Fold axes**	Dykes folded around these same fold axes	Controls dyke orientation & key predictor of dyke trend	Very high
 **Dyke orientation**	Controlled by folding: strike parallel to fold axes and dip approx. mimic dome limbs at km-scales	Determines drillhole orientation and grade continuity	Very high
 **Foliation (S-tectonite planes)**	Defines limbs of domes & basins; dykes dip approximately parallel to dome limbs at the km-scale	Guides dip & orientation of target dykes when working at km-scales in 3D models; correlation progressively becomes less robust at smaller scales	High
 **Axial planes**	Typically upright at regional-scale; locally variable dip at individual outcrops due to constrictional strains	Take care - constrictional strains cause diverse orientations of axial planes at deposit scales	Moderate
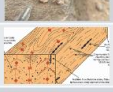 **Regional structural grain**	Dykes, fold axes and lineations dominantly strike NE-SW throughout the southern Central Zone	Take care – heterogeneities locally rotate structures into different orientations e.g. at the MS7 prospect	Moderate
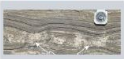 **Boudin necks**	Parallel to lineations, fold axes & dyke strike	Fluids *may* pool in boudin necks (this is untested)	*Unclear*
 **Shear-sense indicators**	Opposite shear senses on opposite dome limbs confirms coaxial strain / pure shear regime	Important for 3D symmetry of structures at km-scales, limited direct applications in exploration or modelling	Low

Abstract

Orogenic pegmatite deposits host critical metals for the energy transition, including lithium, tin, tantalum, and uranium. However, the structural setting of these deposits is not well documented. This hampers exploration and mining, because there is no conceptual framework linking strain patterns to practical applications such as drilling and 3D modelling. In the southern Central Zone of the Damara Orogen, detailed mapping reveals that syn-tectonic dykes are universally strongly folded at all scales (cm to km). The plunge and azimuth of lineations (stretching/rodding/mullions) and minor fold axes reliably informs on the strike of dykes. Axial planes in the folded dykes locally dip at a variety of orientations due to constrictional strains, but the dykes consistently dip parallel to the limbs of dome and basin structures at the km-scale. These consistent field relationships arose because both the dykes and country rocks were folded together during the Damara Orogeny. This conceptual understanding allows limited structural data - obtained from surface mapping, core logging, or geophysical datasets – to reliably guide exploration drilling and 3D geological modelling, thereby reducing missed targets and ensuring tighter mineral resource estimation. The complex regional architecture of the southern Central Zone is best explained by progressive lateral constrictional flow. Melt-driven rheological weakening under granulite facies conditions resulted in pervasive strain distribution. Since the mid-crust was too weak to support further crustal thickening, continued NW-SE shortening was instead accommodated by ductile NE-SW extrusion parallel to the flanks of the orogen. This explains the isobaric heating path to peak granulite-facies metamorphic conditions.

Table of Contents

1) Introduction

Pegmatites and leucogranites are common in the exhumed mid-crustal regions of orogenic belts (e.g., Searle et al., 2010). S-type geochemical signatures suggest that they mostly form via partial melting of metasedimentary source rocks under high temperature regional metamorphic conditions (Nabelek, 2020). Pegmatitic leucogranites host numerous critical mineral deposits including lithium (Balaram et al., 2024), caesium and tantalum (Goodenough et al., 2019), tin (Ashworth et al., 2020), and uranium (Kinnaird and Nex, 2007). The economic importance of these deposits is growing as global net zero policies drive increasing demand for low carbon technologies. Lithium demand for use in electric vehicle batteries is booming, tin demand is growing from the electronics, solar power and electric vehicle industries, and uranium provides the key raw material for low-carbon nuclear power production (International Energy Agency, 2024).

Despite the growing economic importance of orogenic pegmatite deposits, detailed studies on their structural setting remain relatively few (e.g. Silva et al., 2023; Grigson et al., 2025; Koopmans et al., 2025) – particularly in comparison to studies on their geochemistry, petrography and mineralogy (e.g. Cerny and Ercit, 2005; Hill, 2015; London, 2018). The limited structural data available hampers the mining and exploration industry, since there is little conceptual understanding of how pegmatite dykes are distributed and orientated in relation to deformation structures in the host country rocks. This prevents structural mapping of strain patterns (e.g. fold structures, lineations) from being readily translated into practical applications, such as optimising drill hole orientation or improving 3D structural modelling. For other mineral systems – such as orogenic gold – the more mature structural framework available can directly guide exploration activities (e.g., Groves et al., 2018).

This contribution defines the structural and tectonic setting of pegmatite dykes in the former mid-crust of the Damara Orogen. These pegmatites are renowned for world-class uranium mineralisation (Kinnaird and Nex, 2007). Pegmatites further afield in the Damara Orogen host significant tin deposits and lithium mineralisation (e.g., Uis tin mine run by Andrada Mining; see summary of regional pegmatites in Ashworth et al., 2020). This study (1) first documents how the geometry and orientation of leucogranite and pegmatite dykes relates to deformation structures in the host country rocks (especially folding and linear fabrics); (2) discusses how a simple field-based conceptual model can guide practical activities in the mineral exploration and mining industry, and (3) evaluates different structural models for the regional tectonic setting, which provides critical context for the interpretation of structural features at the camp and deposit scales.

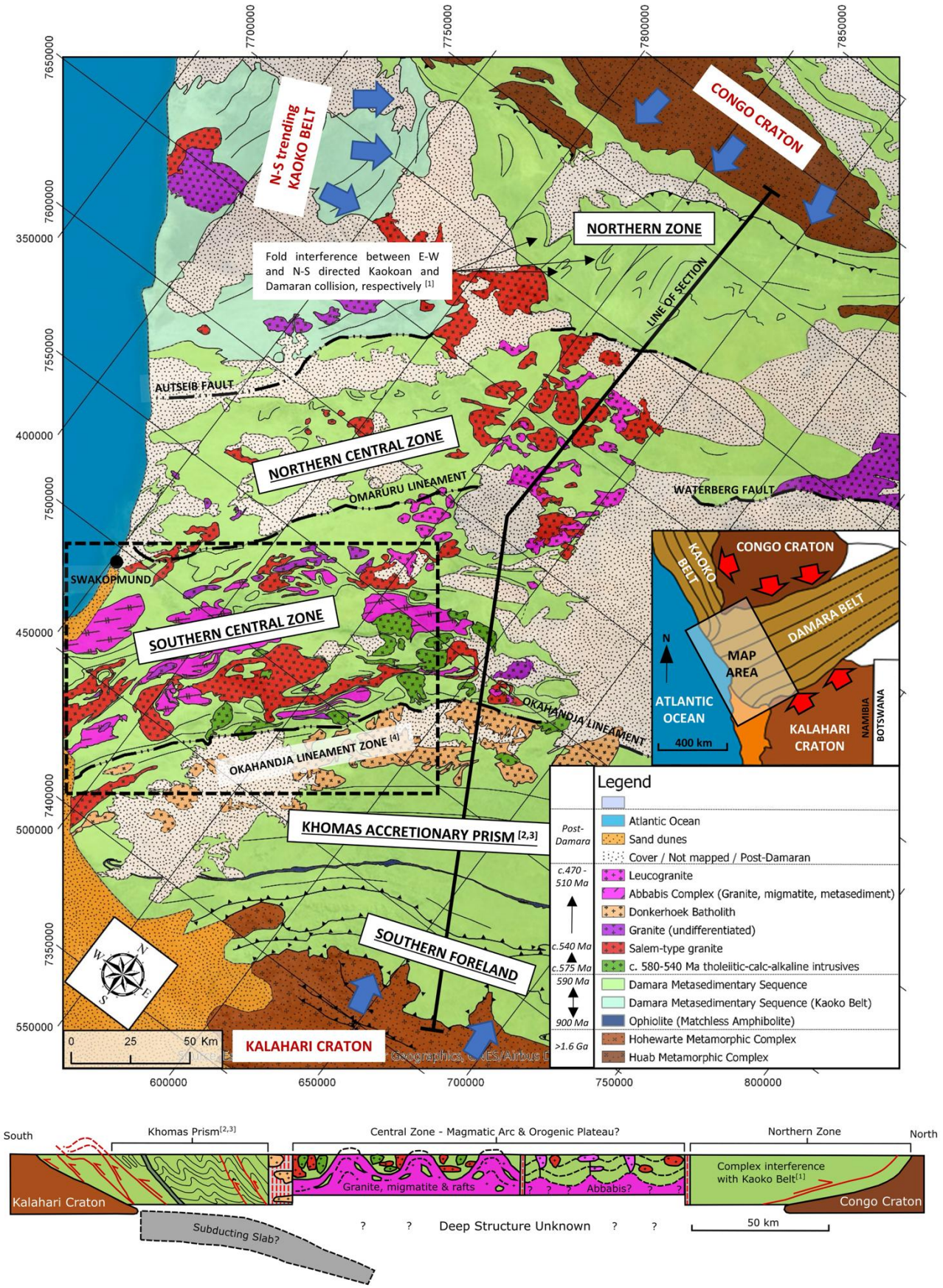

Figure 1 – Regional geological map and interpretative cross-section of the Damara Orogen, modified after Miller and Grote (1988), Geological Survey of Namibia (Sheets 2214, 2216, 2116, 2114, 2014), and Knupp (2019). Note that the Abbabis Complex is traditionally interpreted as c. 1-2 Ga basement in the Central Zone; for its alternative interpretation as an intrusive granite-migmatite complex see Toe et al. (2013) and Jones et al. (2023). The present study focusses on the southern Central Zone.

2) Geological Setting

The Damara Orogen formed from NW-SE collision between the Congo and Kalahari cratons at c. 575 Ma to c. 500 Ma. The orogen has a bivergent structure (Figure 1), consisting of thick and oppositely dipping metasedimentary thrust wedges of the Northern and Southern Zones, which bookend complex fold interference structures and widespread granite magmatism in the Central Zone. Peak metamorphic pressures reached 10.5 kbar and 11.5 kbar in the Northern and Southern zones, respectively (Goscombe et al., 2017), while peak pressures in the southern Central Zone are considerably lower at just 4-5 kbar (Longridge et al., 2017; Jung et al., 2019). This suggests that either crustal thickening was less intense in the Central Zone, or that evidence for earlier crustal thickening was overprinted by later high-temperature and lower-pressure granulite-facies regional metamorphism at c. 520-510 Ma. The latter interpretation is purely speculative, since no evidence for decompression is recorded in the metamorphic data in the run up to peak granulite facies conditions (Longridge et al., 2017; Jung et al., 2019; MacRoberts et al., 2025).

Peak leucogranite and pegmatite magmatism occurred at c. 520-510 Ma in the Central Zone (Jung et al., 2001; Jung and Mezger, 2003; Longridge et al., 2011; Paul et al., 2014; Jung et al., 2014; Longridge et al., 2017; Jung et al., 2019), overlapping with peak high-temperature granulite-facies regional metamorphism (Longridge et al., 2017; Jung et al., 2019). Both leucogranite magmatism and coeval granulite-facies metamorphism lagged the onset of collision by at least ~20-30 Myr, as constrained by the c. 575-540 Ma age of pre- to syn-collisional mafic-to-intermediate plutons (Milani et al., 2015 and references therein; Simon et al., 2017; Schwark et la., 2018; Goslin, 2019; Jung et al., 2020a; Jung et al., 2020b). This 20-30 Myr time lag is consistent with timescales required for radioactive heat production in thickened orogenic crust (Clark et al., 2011; Jaupart et al., 2016). Field, geochemical and isotopic data also indicate that these leucogranites are predominantly S-type and derived from melting of crustal sources (Jung et al., 2001; Ward et al., 2008; Paul et al., 2014; Ashworth et al., 2020).

The southern Central Zone of the orogen consists of two primary rock units. The Abbabis Complex outcrops at the deepest exposed levels in the cores of dome structures. It is a heterogeneous assemblage, comprising of discontinuous rafts and schlieren-like remnants of metasedimentary units, which are universally cross-cut by a volumetrically more abundant assortment of orthogneisses, granitic gneisses, and leucocratic augen gneisses (generally resembling migmatites), and, in places, widespread intrusive granites (Smith, 1965; Marlow, 1981; Barnes, 1981; Sawyer, 1979; Jacob et al., 1983; Brandt, 1987; Longridge, 2012; Jones et al., 2023). The Abbabis Complex is overlain both on the limbs of dome structures, and in intervening synclinoria, by thicker and more coherent metasedimentary units attributed to a Neoproterozoic Damara Supergroup. The age of the Abbabis

Complex and its relationship to the overlying Damara Supergroup is disputed. Traditionally, the Abbabis Complex is interpreted as an older c. 1 or 2. Ga pre-Damaran basement complex, which is unconformably overlain on the dome limbs by the metasedimentary Damara Supergroup (Jacob et al., 1978; Kroner et al., 1991; Tack et al., 2002; Longridge et al., 2018). In contrast, Toe et al. (2013) and Jones et al. (2023) propose that the Abbabis Complex instead represents a syn-orogenic granite-migmatite complex which is intrusive into the overlying Damara Supergroup. In the latter case, the Abbabis Complex is suggested to have formed directly from widespread partial melting and granite intrusion under granulite-facies regional metamorphic conditions in the mid-crust of the Damara Orogen (Jones et al., 2023).

There is no agreement on the structural evolution of the southern Central Zone. Models proposed to explain complex fold interference structures in the region include a single phase of constrictional flow (Poli & Oliver, 2001), diapirism (Barnes & Downing 1979; Barnes, 1981; Kroner, 1984), polyphase deformation with distinct overprinting events (Smith, 1965; Jacob et al., 1983; Longridge et al., 2011; Ormond et al., 2024), tip-line folds above blind thrusts (Kisters et al., 2004; Kruger & Kisters, 2016), and extensional collapse in a model suggested to be analogous to metamorphic core complex formation (Oliver 1994, 1995).

The present study focusses on several dome structures which are well exposed along the lower Swakop River in the southern Central Zone of the orogen (Figure 2). The most detailed mapping was undertaken at the Ida Dome and adjoining synclinoria and structural basins, with reconnaissance structural data and observations also presented from the neighbouring Husabberg Anticlinorium, as well as from some less-well exposed dome structures to the south of the Swakop River (Figure 2). Rock units in the study area comprise of the Abbabis Complex in the cores of the dome structures, and metasedimentary units of the Damara Supergroup on the overlying dome limbs (Figure 2). Leucogranites and pegmatites are widespread throughout both the Abbabis Complex and the overlying metasedimentary Damara Supergroup. Several uranium prospects occur directly in the study area and are shown on the map in Figure 2.

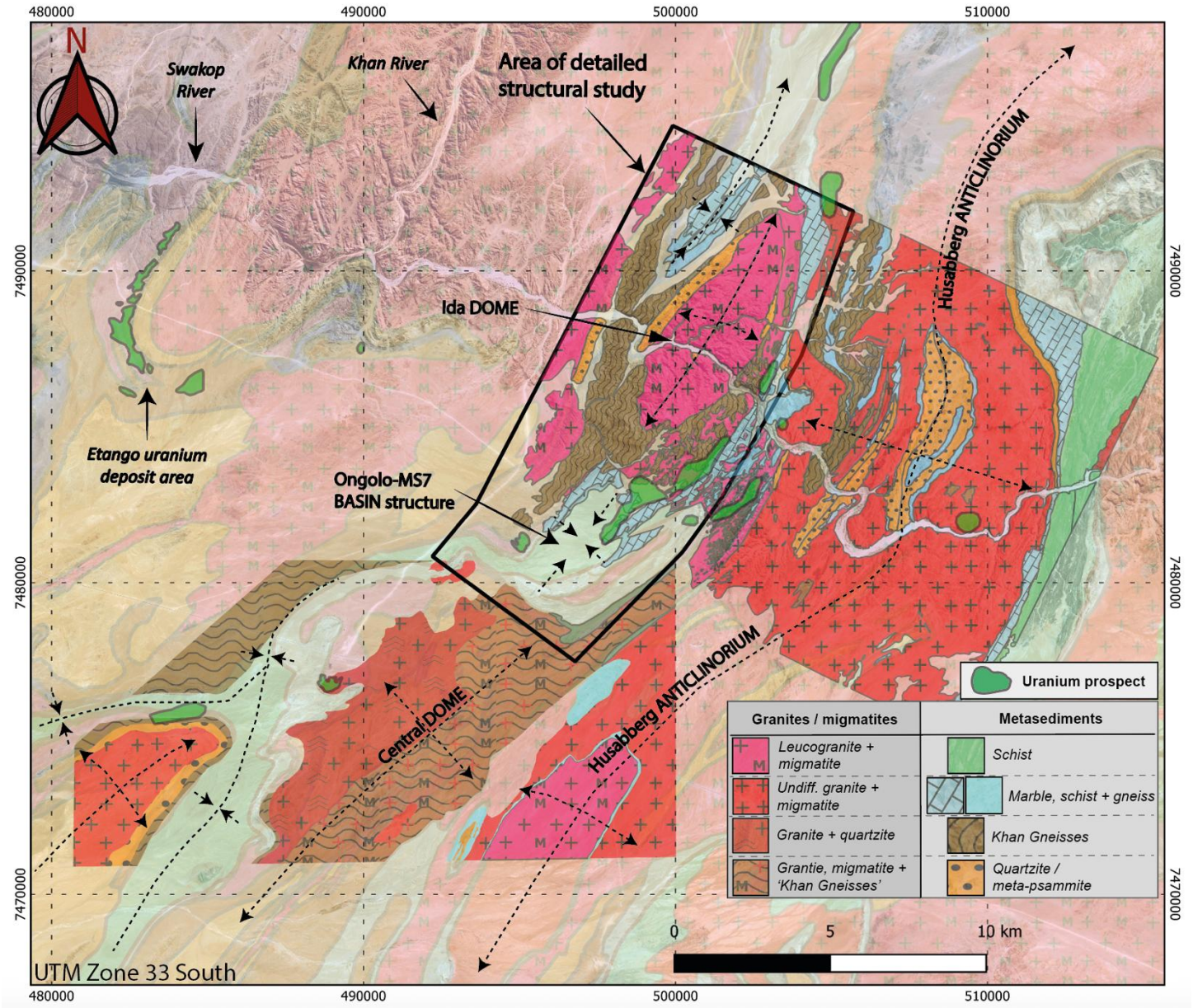

Figure 2 – Local geological map of the study area, centred on the Ida Dome and adjoining dome and basin structures. Solid colour map after Jones (2021) and Jones et al. (2023). Lightly shaded basemap after Knupp (2019). Known uranium deposits and prospects outlined in solid green colour.

3) Results from Field Mapping

3.1 Rock Fabrics: S-tectonites vs L-tectonites

Most rocks in the study area contain both planar and linear fabrics (L-S tectonites). Spatial and compositional variations determine which of these is dominant:

3.2.1 L>S-tectonites

L>S tectonites are common in rocks with a heterogenous composition. Examples include migmatites of the underlying Abbabis Complex (Figure 3A), thinly interlayered (cm-scale) marble and calc-silicate gneiss packages (Figure 3B), and quartz-clinopyroxene-amphibole+/- garnet gneisses (Khan gneisses) (Figure 3C and 3D). L>S tectonites are sometimes accompanied by a mineral and mineral-aggregate stretching lineation at the cm-scale. Many L>S tectonites take on the appearance of "mullions" – particularly in rocks with a heterogeneous composition (Figure 3E-3G).

L>S tectonites are found almost anywhere in the study area, but the strongest examples are frequently observed in heterogenous rock units in the noses of map-scale fold structures e.g., the spectacular metre-scale outcrops in the nose of the MS7 fold structure (Figure 3C and 3D). Strong examples of L>S tectonites are observed both within the underlying Abbabis Complex and in the overlying Damara Supergroup (Figure 3). In contrast to Oliver (1994, 1995), strong L>S tectonites were observed both proximal *and* distal to this contact and are not spatially associated with it.

3.2.2 S>L-tectonites

S>L tectonites are also very common in the study area. S>L tectonites dominate in thicker, more homogeneous, marble units, but they are also common in heterogenous units – particularly where the foliation is orientated parallel to the regional NE-SW trending structural grain. S>L tectonites are frequently associated with tight-to-isoclinal fold structures (Figure 4) which accommodated transposition of earlier rock layering (foliations and/or bedding).

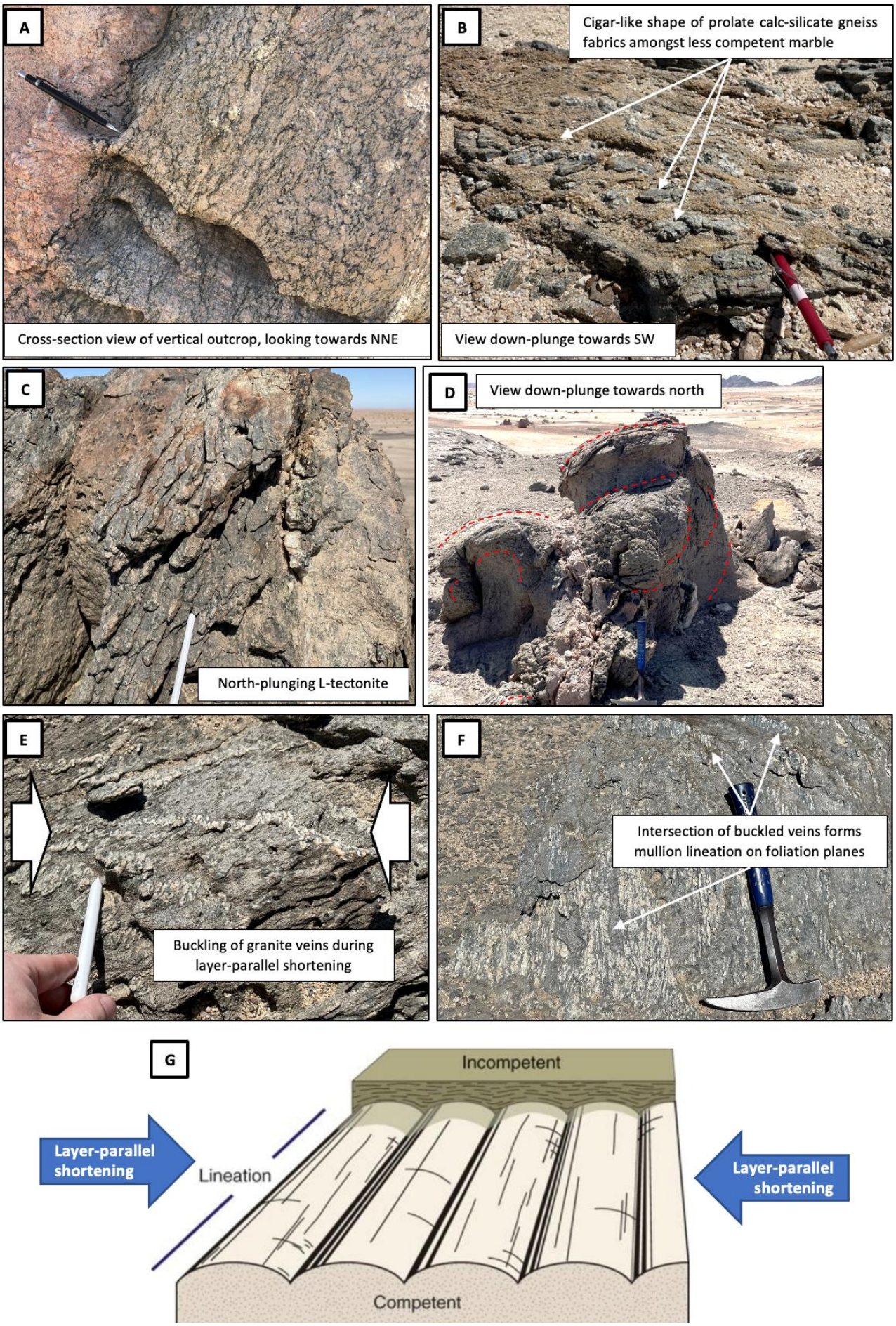

Figure 3 – L-tectonite fabrics in the study area. A) Migmatites of the Abbabis Complex, western edge of the Husabberg Anticlinorium. B) Within thinly interlayered marble and calc-silicate gneisses in the Ongolo area to the SW of the Ida Dome. C and D) At the cm- and metre-scale in the core of the MS7 fold structure. E and F) Mullion lineations formed by buckling of competent leucogranite veins/dykes within a ductile matrix. G) Schematic illustration of mullion lineation formation, modified slightly from Fossen (2016).

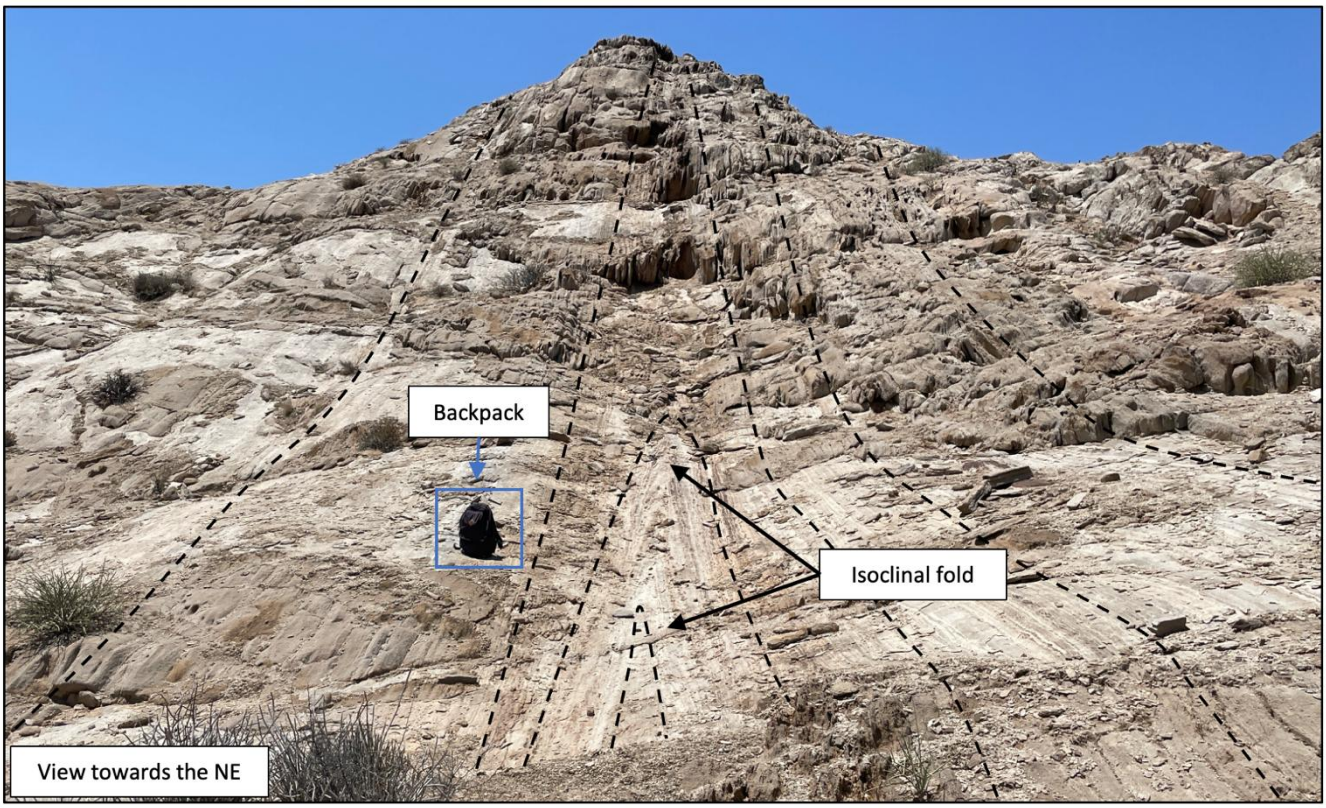

Figure 4 – S-tectonite fabrics in marble units at the Gurtel Hills Synform.

3.2 Fold Structures: Country rocks (metasedimentary Damara Supergroup)

3.2.1 Upright NE-SW striking folds

Across all areas, structural data plotted on stereonets reveals predominantly upright folding at the km-scale, with no consistent vergence to either the NW or SE:

- At the Ida Dome, poles to foliation planes reveal that both the NW and SE limbs dip moderately to steeply, consistent with an overall upright NE-SW trending fold structure (Figure 5A).
- To the west of the Ida Dome, poles to foliation planes for the Zebraberg-Southberg Synform and Gurtel Hills Synform also define two moderately-dipping limbs which reflect an upright NE-SW trending synform (Figure 5A).
- The Husabberg Anticlinorium to the east of the Ida Dome reveals comparable moderately WNW and ESE-dipping limbs, consistent with another upright fold structure striking NNE-SSW (Figure 5B).

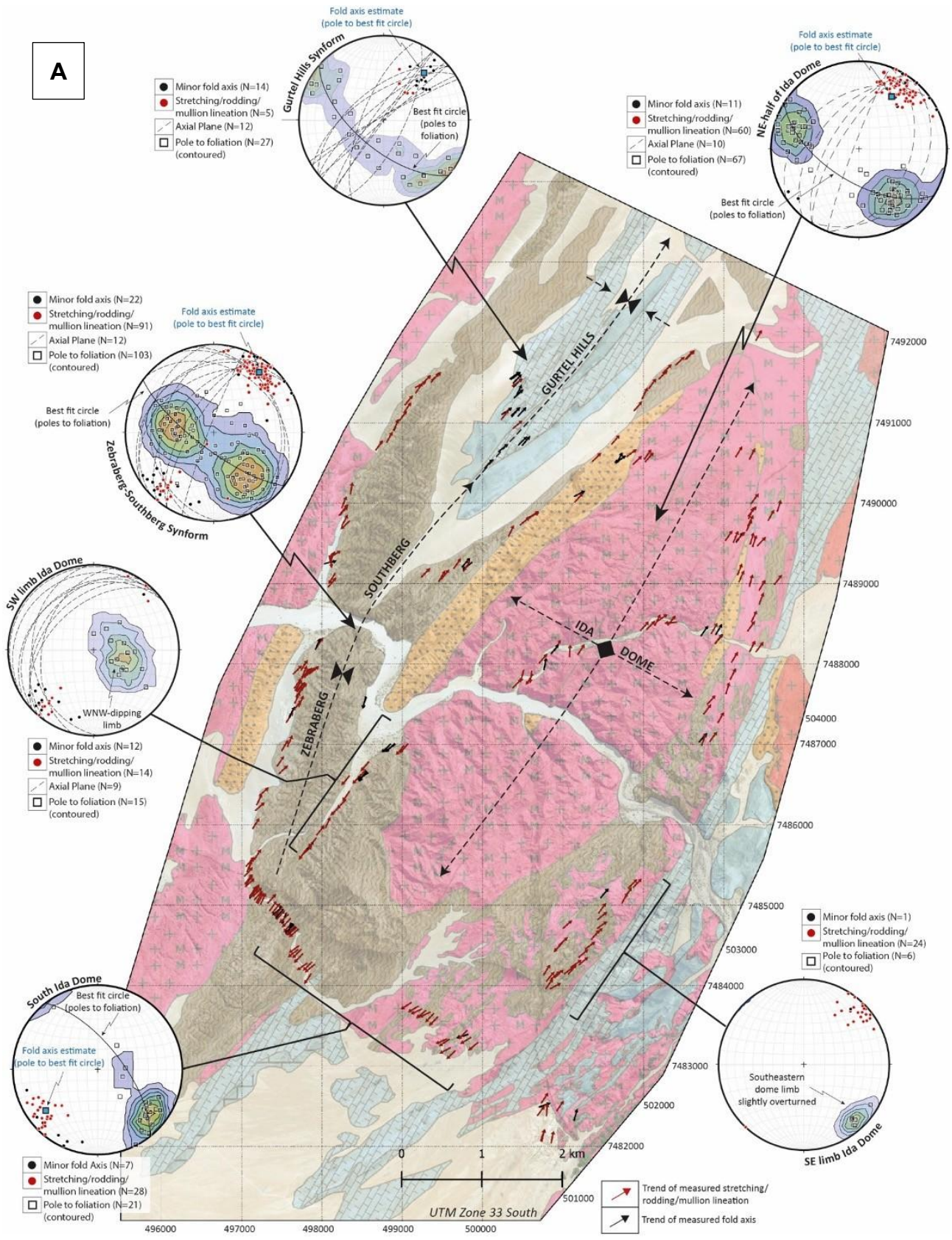

Figure 5 – Structural data for foliations, lineations, fold axes, and fold axial planes. A) At the Ida Dome. B) At other dome structures surrounding the Ida Dome, including the Husabberg Anticlinorium, the Central Dome, and the Northern Twin Hills Basin. C) At the Ongolo-MS7 Basin between the Ida Dome to the NE and the Central Dome to the SW. For lithological legend see Figure 2.

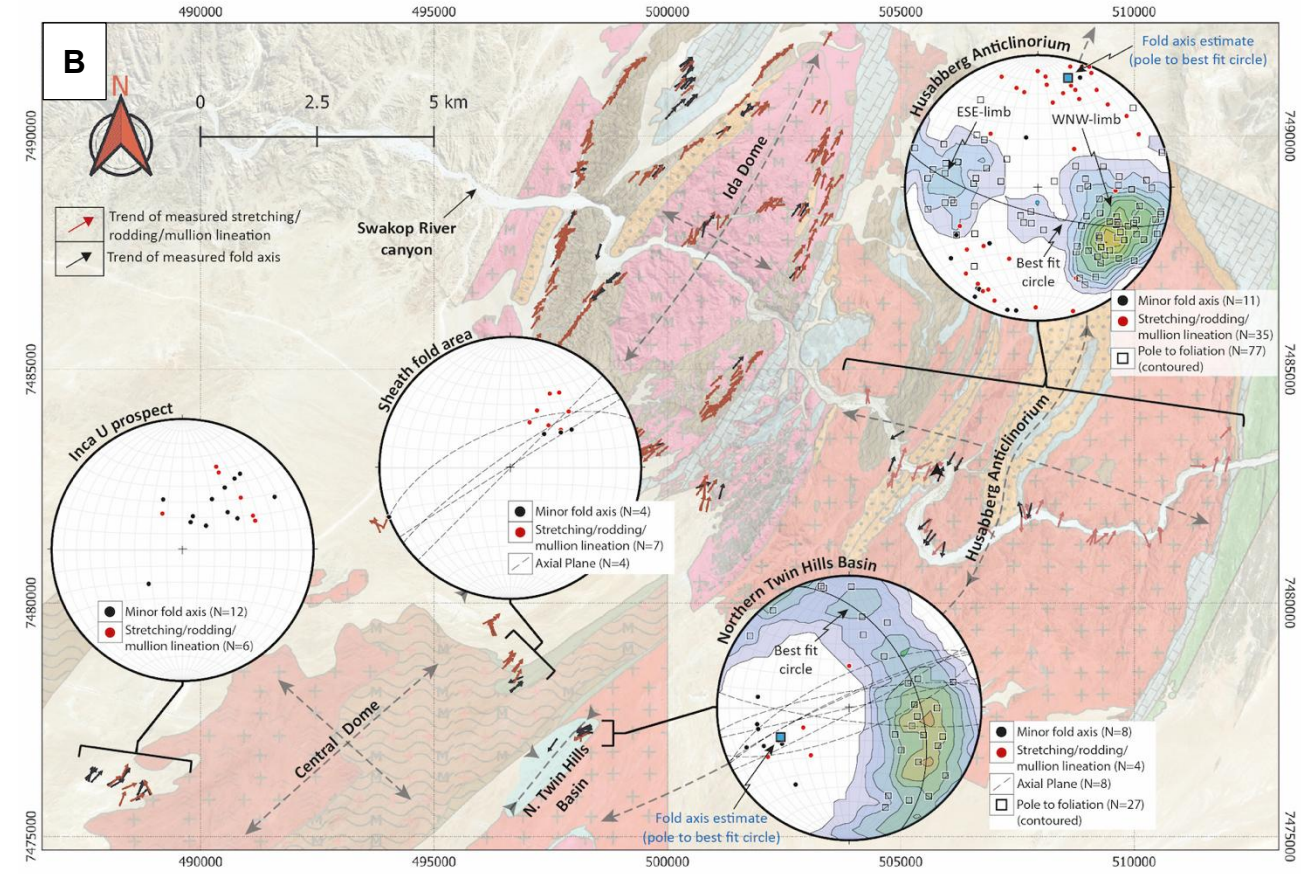
B
N
0
2.5
5 km
Trend of measured stretching/ rodding/mullion lineation
Trend of measured fold axis
Swakop River canyon
Ida Dome
Husabberg Anticlinorium
Fold axis estimate (pole to best fit circle)
ESE-limb
WNW-limb
Best fit circle
Minor fold axis (N=11)
Stretching/rodding/ mullion lineation (N=35)
Pole to foliation (N=77) (contoured)
Sheath fold area
Minor fold axis (N=4)
Stretching/rodding/ mullion lineation (N=7)
Axial Plane (N=4)
Inca U prospect
Minor fold axis (N=12)
Stretching/rodding/ mullion lineation (N=6)
Central Dome
N. Twin Hills Basin
Northern Twin Hills Basin
Best fit circle
Minor fold axis (N=8)
Stretching/rodding/ mullion lineation (N=4)
Axial Plane (N=8)
Pole to foliation (N=27) (contoured)
Fold axis estimate (pole to best fit circle)
490000
495000
500000
505000
510000
7490000
7485000
7480000
7475000

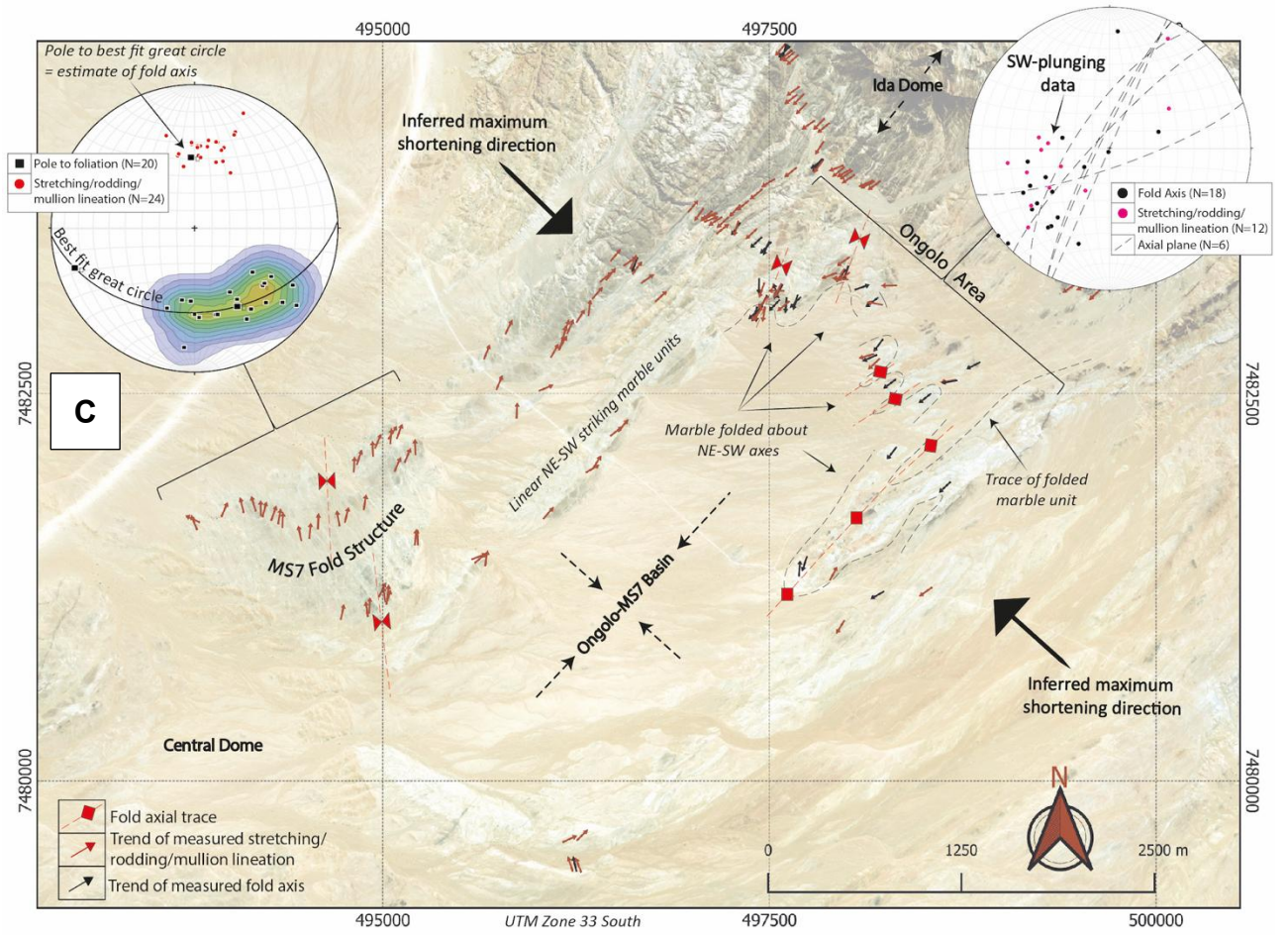
C
Pole to best fit great circle = estimate of fold axis
Pole to foliation (N=20)
Stretching/rodding/ mullion lineation (N=24)
Best fit great circle
Inferred maximum shortening direction
Ida Dome
SW-plunging data
Fold Axis (N=18)
Stretching/rodding/ mullion lineation (N=12)
Axial plane (N=6)
Ongolo Area
Linear NE-SW striking marble units
Marble folded about NE-SW axes
Trace of folded marble unit
MS7 Fold Structure
Ongolo-MS7 Basin
Inferred maximum shortening direction
Central Dome
Fold axial trace
Trend of measured stretching/ rodding/mullion lineation
Trend of measured fold axis
N
0
1250
2500 m
UTM Zone 33 South
495000
497500
500000
7482500
7480000

3.2.2 Secondary folding & crenulations

Secondary crenulation-style folding is common where rocks strike perpendicular to the regional NE-SW trending structural grain, particularly at the inflection points on the NE and SW hinge zones of dome and basin structures. It is observed across several scales ranging from outcrop- to map-scale:

- *At the map-scale*: In the Ongolo area, marble units on the SW hinge zone of the Ida Dome are locally rotated into a 1st-order NW-SE strike (Figure 5C). This NW-SE strike lies perpendicular to the dominant NE-SW structural grain. Subordinate 2nd-order fold structures have developed in these rocks, with inset stereonet data in Figure 5C revealing these to have upright axial planes striking consistently NE-SW. These 2nd-order NE-SW oriented fold structures restore parallelism with the regional structural grain (Figure 5C).
- *At the outcrop-scale*: Similar crenulation-style folds to those described above are also observed at the outcrop scale in the hinge zone of the 'Northern Twin Hills Basin' (Figure 6A).

3.2.3 *Km-scale domes & basins are doubly plunging towards the NE and SW*

The fold axes of km-scale dome and basin structures are statistically defined on stereonets by the pole to best-fit great circles drawn through pole-to-foliation data. Stereonet data indicates that km-scale fold structures are doubly-plunging to both the NE and SW:

- At the Ida Dome, poles to the great circles (marked by a blue square on the stereonets) consistently define very shallowly NE or SW-plunging fold axes (Figure 5A).
- Shallowly NNE or SSW-plunging fold axes are also defined for the neighbouring Husabberg Anticlinorium to the east of the Ida Dome (Figure 5B)
- The Northern Twin Hills Basin located further south also reveals the same pattern of shallowly SW-plunging fold axes (Figure 5B).

In addition, outcrop-scale fold axes measured directly in the field consistently have the same shallow NE or SW-directed plunge; this mimics the plunge and azimuth of the larger km-scale dome-and-basin structures (Figure 5). The same shallow NE and SW-directed plunge can also be inferred from the intersection of NW- and SE-dipping minor fold axial planes on some of the stereonets (Figure 5).

3.2.4 Lineation data

Linear fabric elements in rocks – in the form of stretching lineations, constrictional rodding lineations, and mullion lineations – have a consistently shallow NE or SW-directed plunge throughout the study area. This mimics the plunge and azimuth of the larger doubly-plunging km-scale dome-and-basin structures described above. This is observed at the Ida Dome (Figure 5A) and in all neighbouring dome structures (Figure 5), although the orientation differs at the MS7 area (discussed below).

3.2.5 Different orientation of the MS7 fold

It is noted that the ~1km wavelength MS7 fold structure, situated between the Ida Dome and the Central Dome, has a slightly different orientation to the dominant NE-SW trend of other folds in the study area. The pole to the best-fit great circle through foliation data defines a moderately north-plunging axis for this fold structure (compared to the NE-SW plunge of neighbouring fold structures) (Figure 5C). Outcrop scale stretching/rodding/mullion lineations in the MS7 area correspondingly also plunge moderately to the north, maintaining their parallelism to the plunge of the 1st-order map-scale fold structure.

3.2.6 *Other quirks and anomalies*

A metre-scale sheath fold was observed in an outcrop near the Ongolo-MS7 basin area, near the NE edge of the ‘Central Dome’ (Figure 6D and 6E).

3.2.7 *Summary*

The overall structural pattern in the metasedimentary country rocks is of one of predominantly upright km-scale folding striking between NNE-SSW and NE-SW; there is no evidence for a consistent vergence to either the NW or SE (Figure 5). Fold axes in metasedimentary units at all scales, ranging from outcrop-scale folds up to km-scale dome-and-basin structures, are consistently shallowly doubly plunging to both the NE and SW (Figures 5). Linear fabric elements in the rocks – in the form of stretching lineations, constrictional rodding lineations, and mullion lineations – consistently plunge in an orientation parallel to the axes of the 1st order map-scale (km-scale) dome-and-basin structures (Figure 5). It is noted that the MS7 fold structure represents an unusual

quirk/anomaly in the fact that it plunges towards the north rather than to the NE or SW (Figure 5C), yet the general relationship of linear fabric elements plunging parallel to the 1st-order fold axes remains true (Figure 5C).

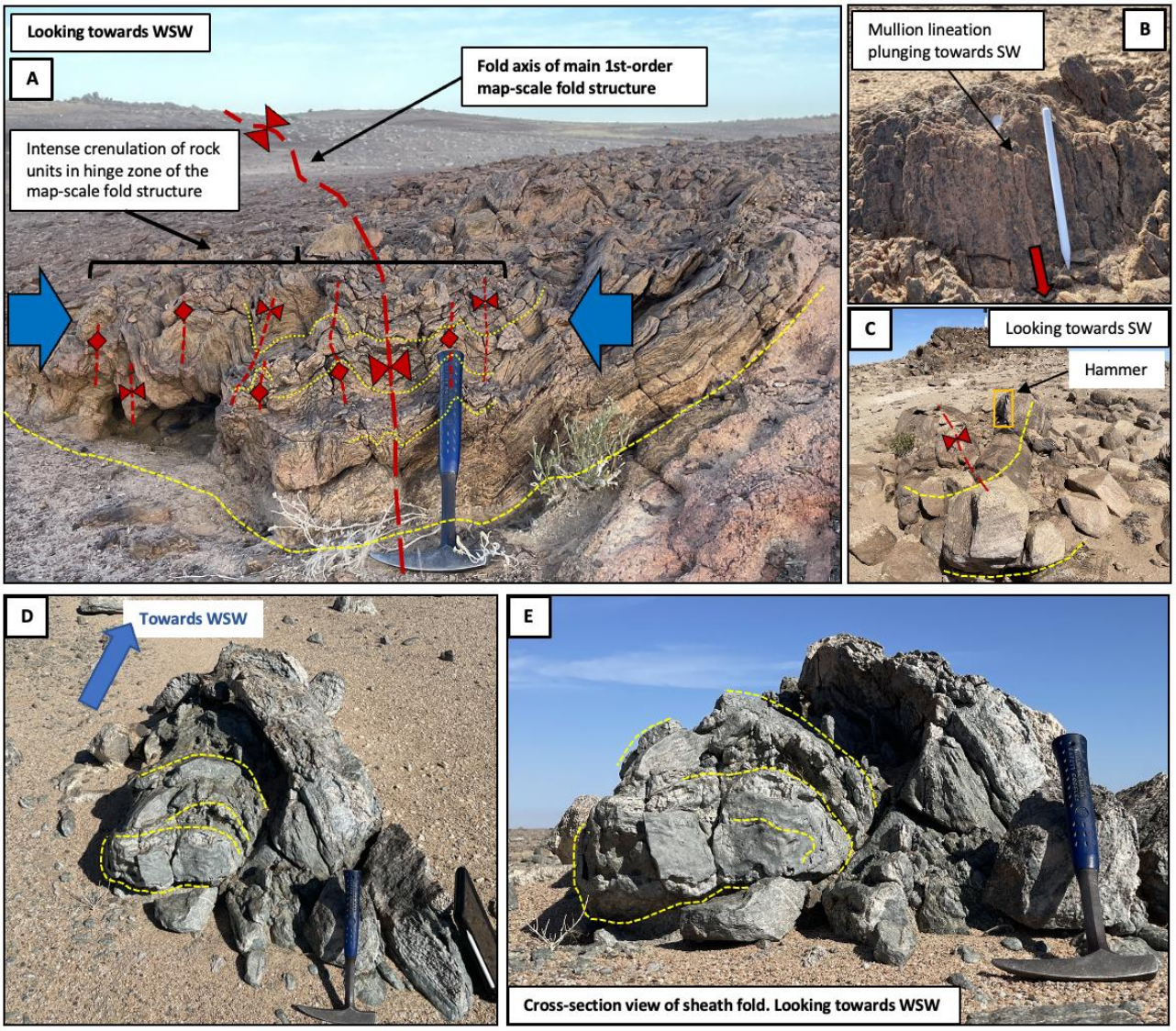

Figure 6 – Examples of fold structures in the country rocks. A) Upright crenulation folding of gneiss in the nose of the Northern Twin Hills Basin. B) The crenulation folding is associated with a mullion lineation in migmatitic units. C) Gently SW-plunging folds with tight to isoclinal limbs in marble units near the northeastern nose of the Northern Twin Hills Basin. D and E) Relatively rare example of a sheath fold, situated at the intersection of the Central Dome and the Ongono-MS7 Basin.

3.3 Fold Structures: Leucogranites and migmatites

3.3.1 Description of folded leucogranites and migmatites in the Abbabis Complex

Figure 7 shows examples of folds within the migmatites and larger leucogranites of the Abbabis Complex in the core of the Ida Dome. Folding occurs at a range of scales, from the mm, to cm, and metre-scale. In most places, fold axial planes are typically steeply dipping to upright, but sub-horizontal axial planes are also locally observed (Figure 7B). Fold axes plunge consistently shallowly to either the NE or SW, mimicking those described above in the metasedimentary country rocks. These field observations are consistent throughout the Abbabis Complex in the core of the Ida Dome.

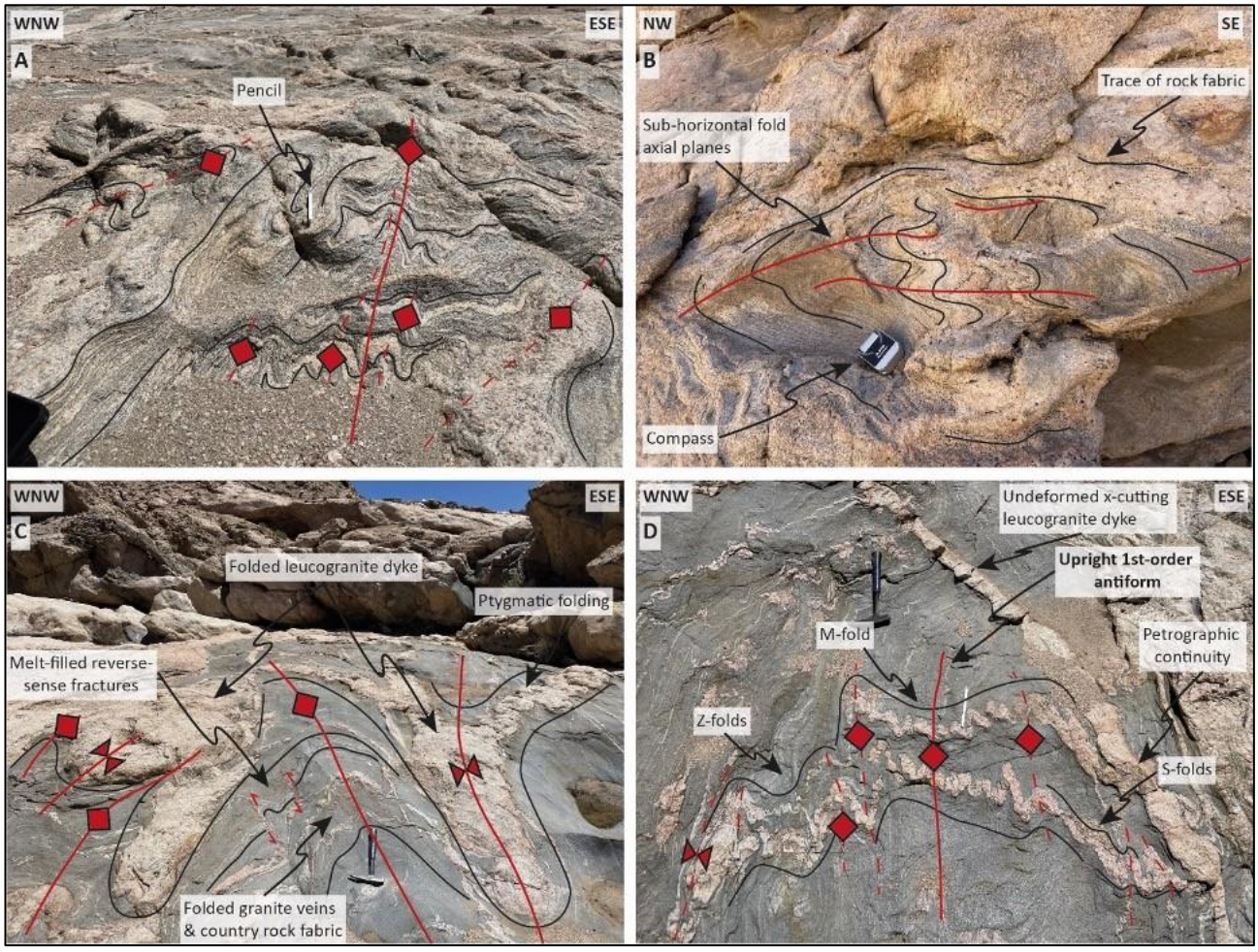

Figure 7 – Folded leucogranite dykes and migmatites in the Abbabis Complex in the core of the Ida Dome.

3.3.2 Description of folded leucogranites in Damara metasediments on the dome limbs

More coherent metasedimentary units are well-exposed in the core of the Zebraberg-Southberg Synform, where they structurally overlie the Abbabis Complex in the core of the Ida Dome. Leucogranite dykes intrude into and cross-cut the foliation in these metasediments at a variety of angles. Careful examination shows that the majority of these leucogranite dykes are folded. Fold axial planes in the leucogranites vary from predominantly steeply-dipping (Figure 8A and 8B) to locally sub-horizontal (Figure 8C). Figure 8D provides a cross section view across the hinge zone of the NE-SW trending km-scale Zebraberg-Southberg Synform – note how the leucogranite dykes have been folded into an upright NE-SW trending synform structure which closely resembles the geometry of the upright 1st order map-scale Zebraberg-Southberg Synform in the host metasedimentary country rocks (shown on stereonet in Figure 5A); this is despite the fact that the dykes themselves clearly cross-cut the synformally-folded foliation of the host country rocks (Figure 8D).

While leucogranite dykes are clearly and consistently strongly folded when observed in the NW-SE plane (e.g., Figure 8), the same dykes frequently lack any obvious folding when observed in the NE-SW plane. This is apparent in the cliff section shown in Figure 9A and is a consistent observation throughout the study area.

Additional observations of leucogranite intrusions into metasedimentary units on the western limb of the Ida Dome are shown in Figure 9. Leucogranites are universally folded; while these folds may locally verge towards the hinge line of km-scale dome structures (Figure 9B), elsewhere axial planes show a wide variety of dip angles (Figure 9C and 9D). The intersection of folded leucogranites with foliation planes results in widespread mullion lineations throughout the study area (e.g. Figure 9B).

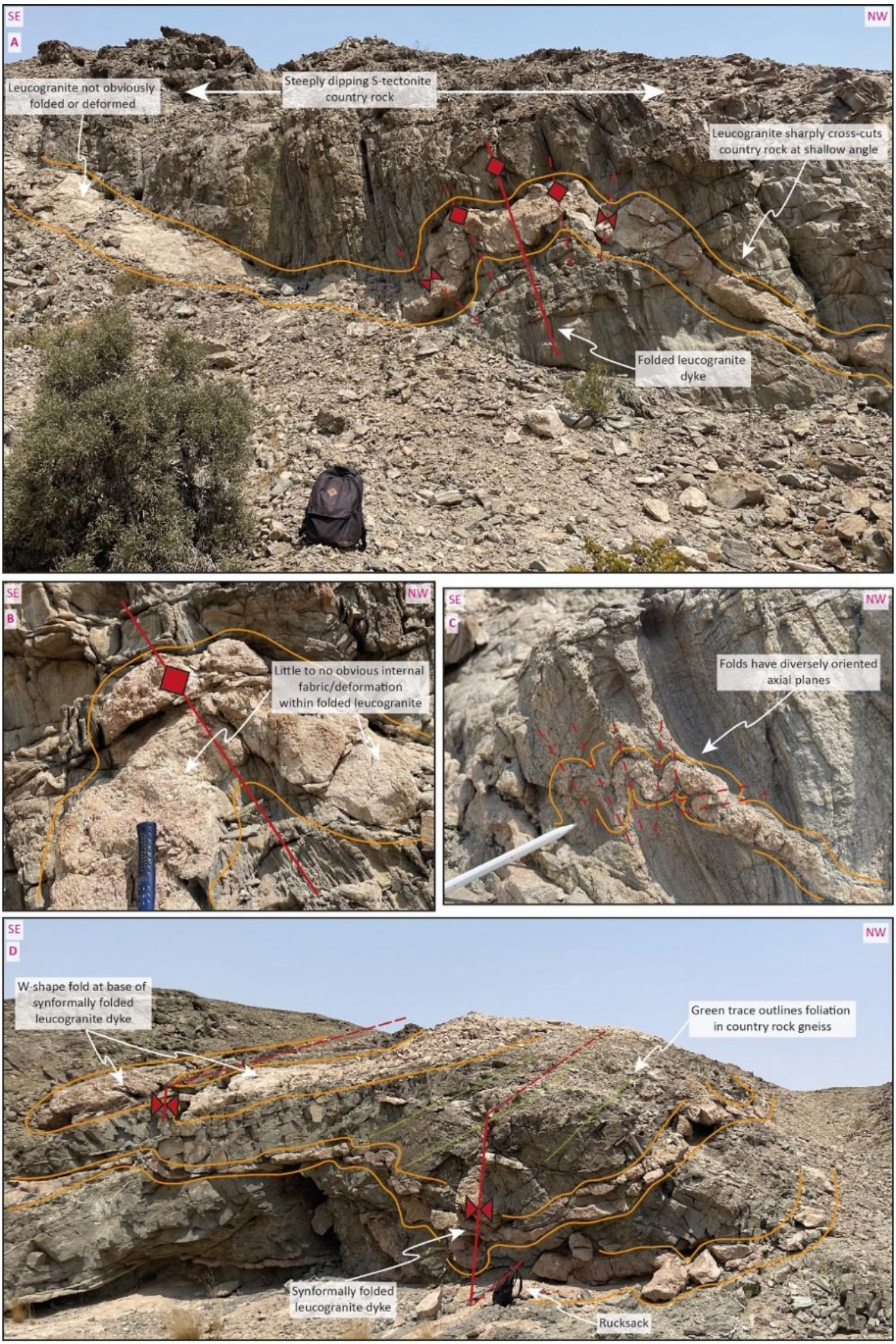

Figure 8 – Folded leucogranite dykes intruding into Khan Gneisses at the Zebraberg Southberg Synform

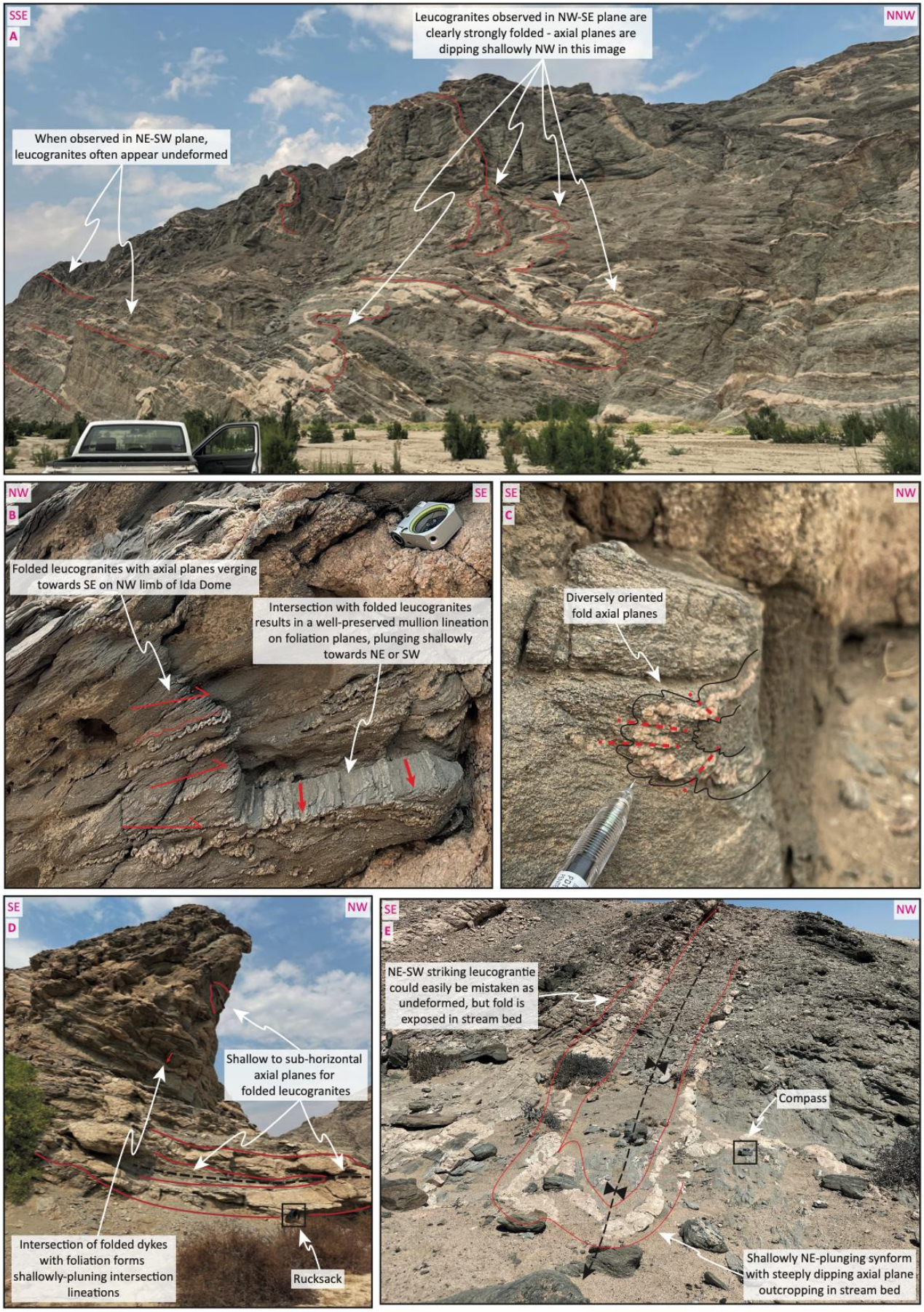

Figure 9 – Folded leucogranite dykes intruding into Khan Gneisses on the NW limb of the Ida Dome

3.3.3 Description of folded leucogranite dykes at larger scales (hundreds of metres up to km-scale)

Figure 10 shows folded leucogranite dykes at the hundreds-of-metres-scale. These dykes intruded into quartz-diopside-amphibole "Khan" gneisses on the SE limb of the Ida Dome; here, they have been folded into a similar NE-SW strike, and their fold axes again plunge consistently towards the NE at a shallow angle.

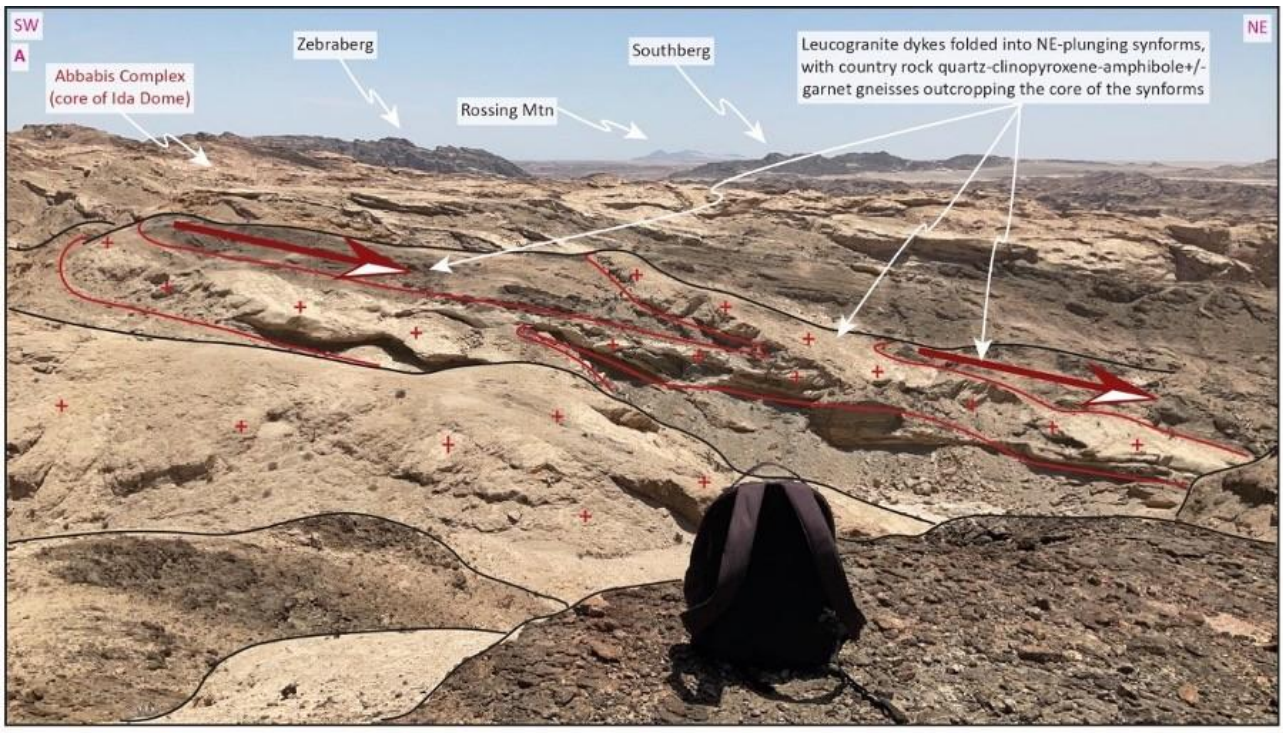

Figure 10 – Folded leucogranite dykes at the hundreds of metres scale on the SE limb of the Ida Dome

3.3.4 Structural dataset for leucogranite intrusions in the study area

Upright km-scale anticlinoria and synclinoria: Structural data for leucogranite dykes at the Ida Dome are plotted on the map and stereonets in Figure 11A. Leucogranite contacts define two distinct clusters on the stereonets – dipping to both the NW and SE; this is clearly visible in the NE portion of the Ida Dome, in the area surrounding the Gurtel Hills Synform, and to the SE of the Ida Dome (Figure 11A) (*note that these two clusters are less distinct on the stereonets in the Zebraberg Synform area (Figure 11A) due to the data having been collected predominantly along the hinge line of the NNE-plunging Zebraberg Synform with insufficient data from the limbs of this synform*). These two clusters again represent the NW and SE-dipping limbs of upright km-scale anticlinoria and synclinoria, indicating that the same pattern of folding described in the field photos above (Figures 7-10) is also apparent at the scale of the entire Ida Dome (4-5 km wavelength). Reconnaissance structural data from the neighbouring Husabberg Anticlinorium reveals a similar macro-scale structural pattern, with both fold limbs dipping to the WNW and ESE (Figure 11B).

Doubly-plunging towards the NE & SW: Furthermore, when a best-fit great circle is drawn through the poles to the leucogranite contacts on each of the stereonets, the pole to this great circle (represented by a blue square on the stereonets) defines fold axes plunging consistently shallowly to either the NE or SW (Figure 11A). This is also the case in the neighbouring Husabberg Anticlinorium, where the implied fold axis plunges shallowly NNE (Figure 11B).

North-plunging at the MS7 area: Here, the fold axis inferred from the best-fit great circle drawn through the poles to leucogranite contacts plunges moderately towards the north (Figure 11C). This retains parallelism to the north-plunging map-scale fold structure in the MS7 area (Figure 5C), which is oblique to the NE-SW trending structural grain of neighbouring folds.

3.3.5 Summary of data & observations on folded leucogranite dykes

In summary, data on the stereonets in Figure 11 defines two distinct fold limbs for the leucogranites in the study area, dipping to the NW and SE. These folds are predominantly upright and do not verge consistently to either the NW or SE at the scale of the study area. Map-scale structural data indicates that these folds plunge consistently shallowly to either the NE or SW. The pattern of folding in these leucogranite dykes is almost identical to the fold pattern described above in the host country rocks (Figure 5).

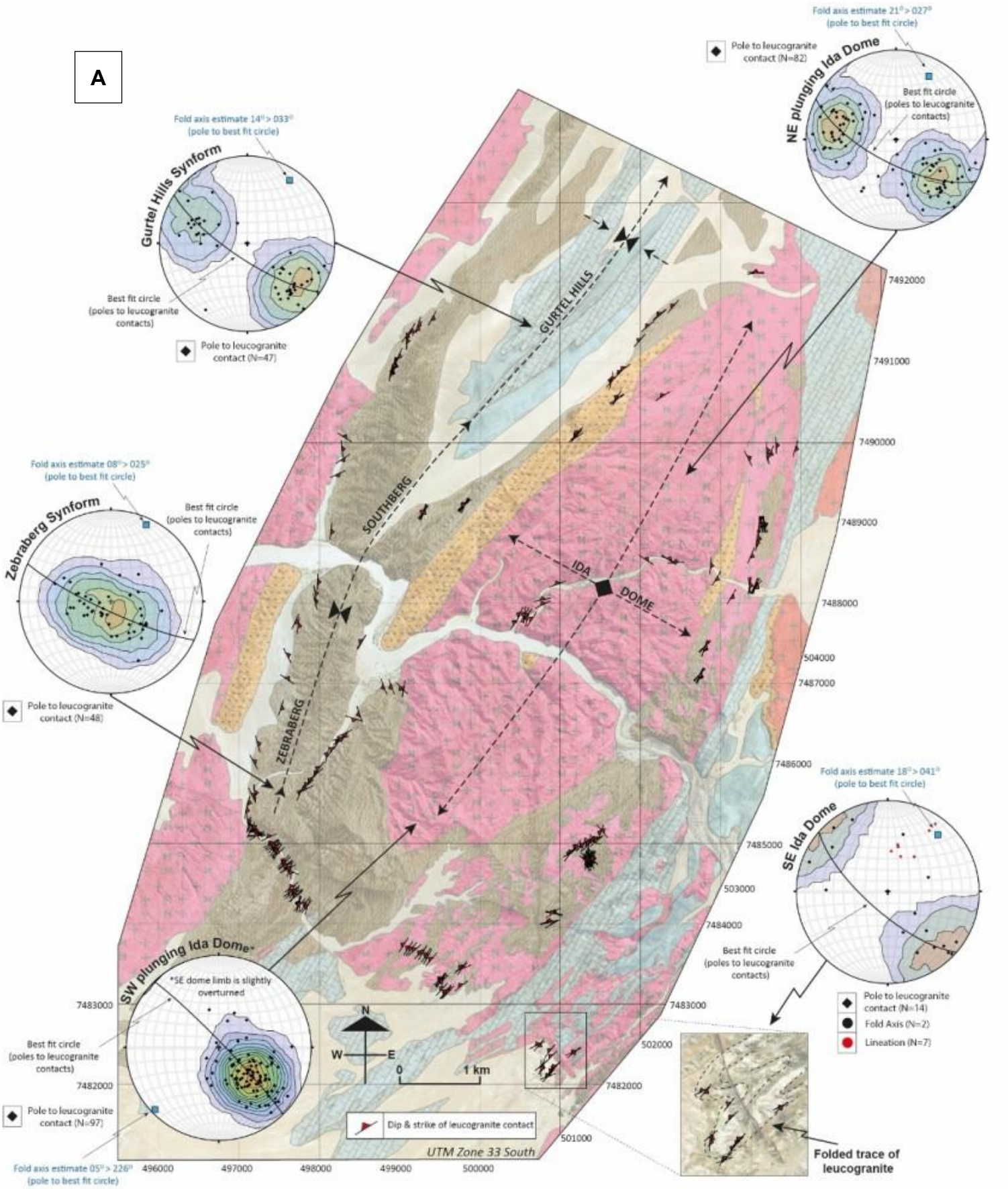

Figure 11 – Structural data for contacts between leucogranite dykes and country rocks. A) At the Ida Dome and Zebraberg-Southberg-Gurtell Hills Synform. B) At the Husabberg Anticlinorium. C) At the MS7 area. For lithological legend see Figure 2.

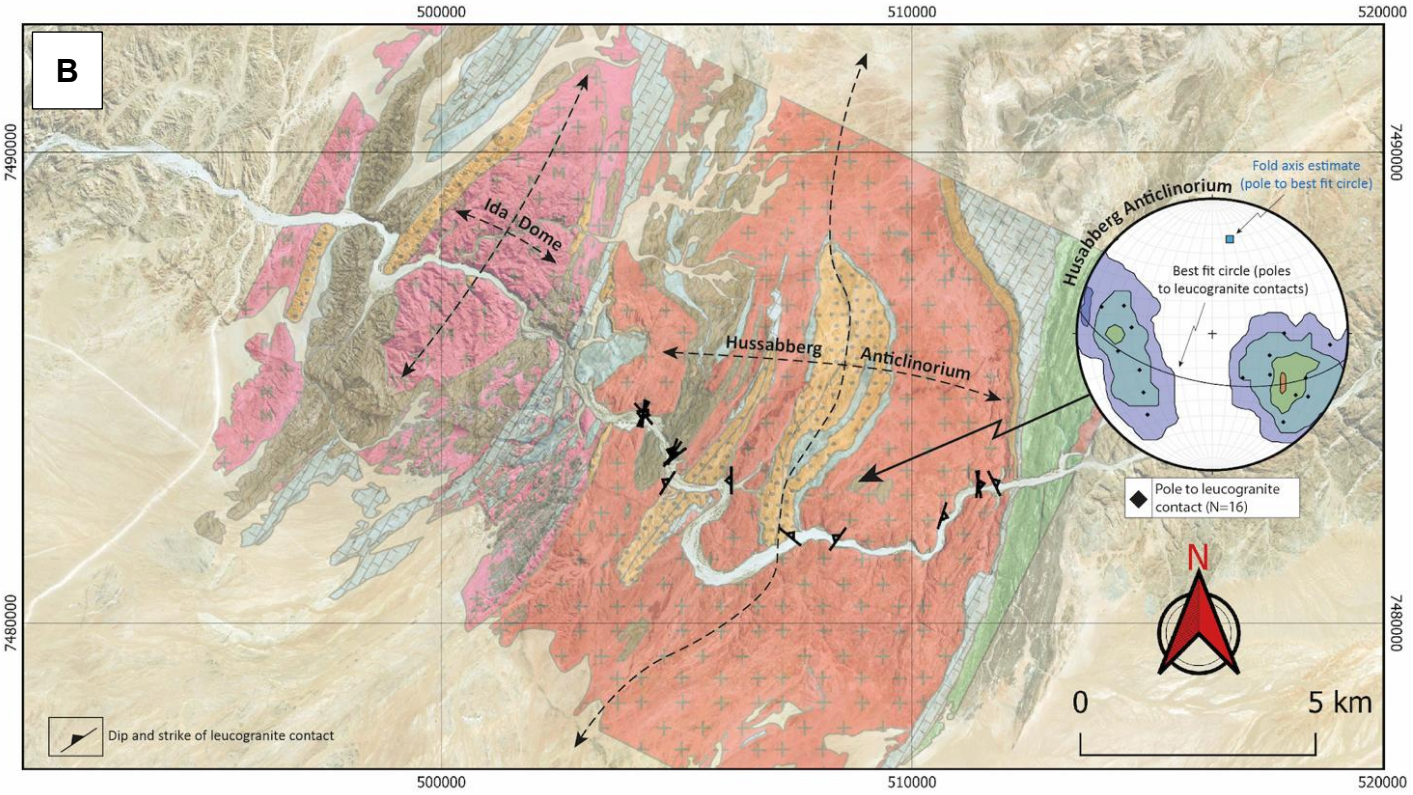
B
500000
510000
520000
7490000
7480000
Ida Dome
Hussabberg
Anticlinorium
Hussabberg Anticlinorium
Fold axis estimate
(pole to best fit circle)
Best fit circle (poles
to leucogranite contacts)
Pole to leucogranite
contact (N=16)
N
0
5 km
Dip and strike of leucogranite contact

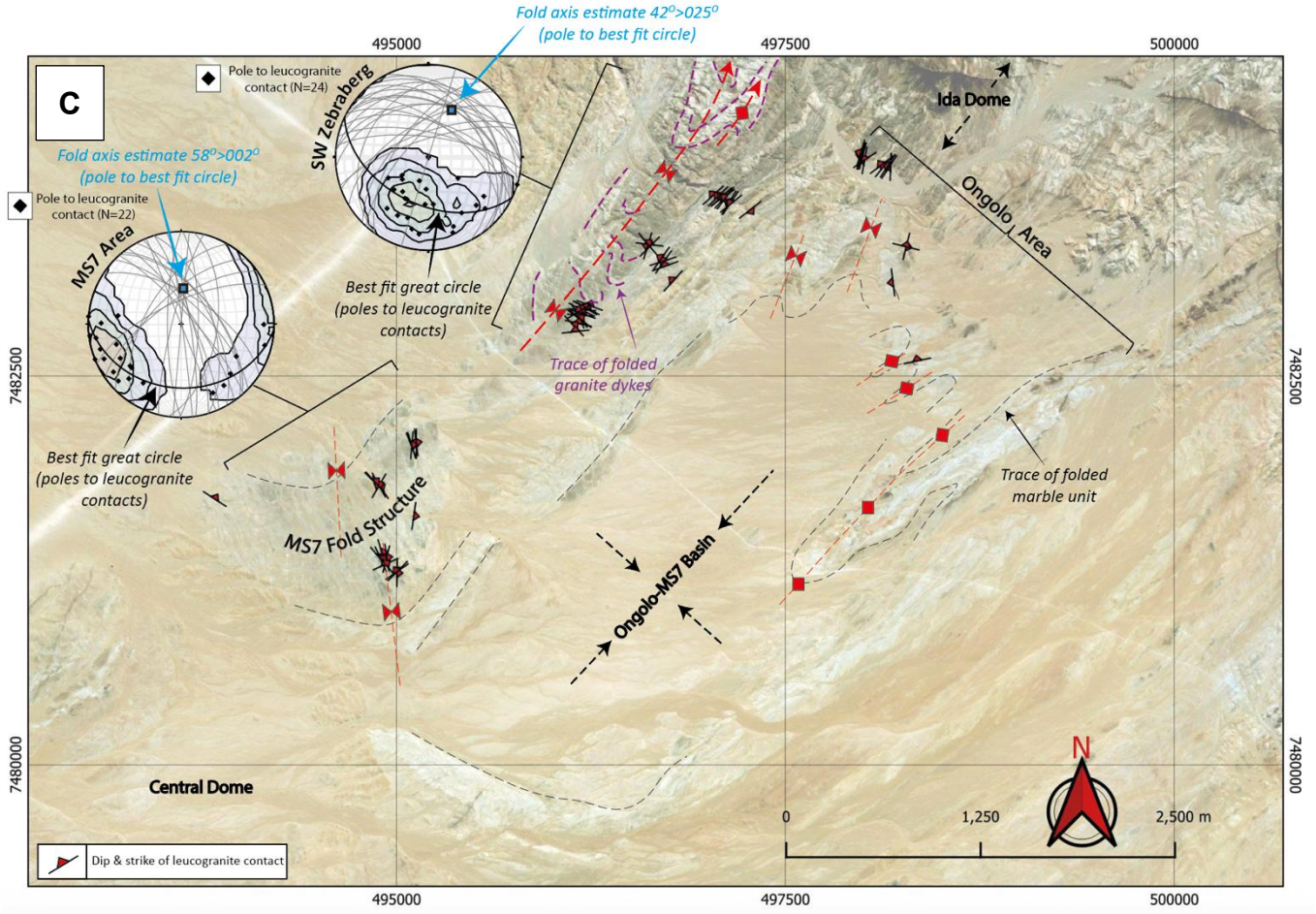
C
Fold axis estimate 42°>025°
(pole to best fit circle)
Pole to leucogranite
contact (N=24)
SW Zebraberg
Best fit great circle
(poles to leucogranite
contacts)
Fold axis estimate 58°>002°
(pole to best fit circle)
Pole to leucogranite
contact (N=22)
MS7 Area
Best fit great circle
(poles to leucogranite
contacts)
Trace of folded
granite dykes
Ida Dome
Ongolo Area
Trace of folded
marble unit
MS7 Fold Structure
Ongolo-MS7 Basin
Central Dome
N
0
1,250
2,500 m
Dip & strike of leucogranite contact
495000
497500
500000
7482500
7480000

3.4 Melt-filled fractures and boudinage

3.4.1 Melt-filled fractures

Systematic sets of elongate lens-shaped leucosomes are developed in more massive and competent quartz-diopside-amphibole+/-garnet gneisses ("Khan Gneisses") throughout the study area (Figure 12). The leucosomes have diffuse boundaries with the host country rock and lack sharp contacts (Figure 12). When observed in plan-view, these leucosome lenses form systematic sets with their long axes consistently oriented ~orthogonal to both the axes of 1st-order map-scale fold structures and to stretching/rodding/mullion lineation in the rocks (Figure 12). They are also consistently oriented ~orthogonal to the stretching direction implied by boudinage structures (e.g. Figure 12A). In places, these features can subtly resemble conjugate sets (Figure 12A). The term "fracture" is used here in a crude descriptive sense since surrounding granulite-facies conditions would inhibit true brittle fracturing; these features likely formed instead via ductile dilation as indicated by the diffuse contacts between the melt portions and surrounding country rock.

3.4.1 Melt-filled boudin necks

Boudinage structures are well-developed in heterogenous rock units with strong competency contrasts throughout the study area; competent calc-silicate units interlayered with marbles provide some of the best examples. Boudinage is also readily observed in the banded Khan Gneisses (Figure 12A), and sometimes in leucogranite dykes and sills intruding into less competent units such as schists. Diffuse melt-filled pockets commonly occupy the neck-zones of boudins (Figure 12C). The stretching direction implied by boudinage is consistently oriented parallel to the subhorizontal stretching/rodding/mullion lineation in the rocks, and parallel to map-scale fold axes i.e. typically in a NE-SW orientation.

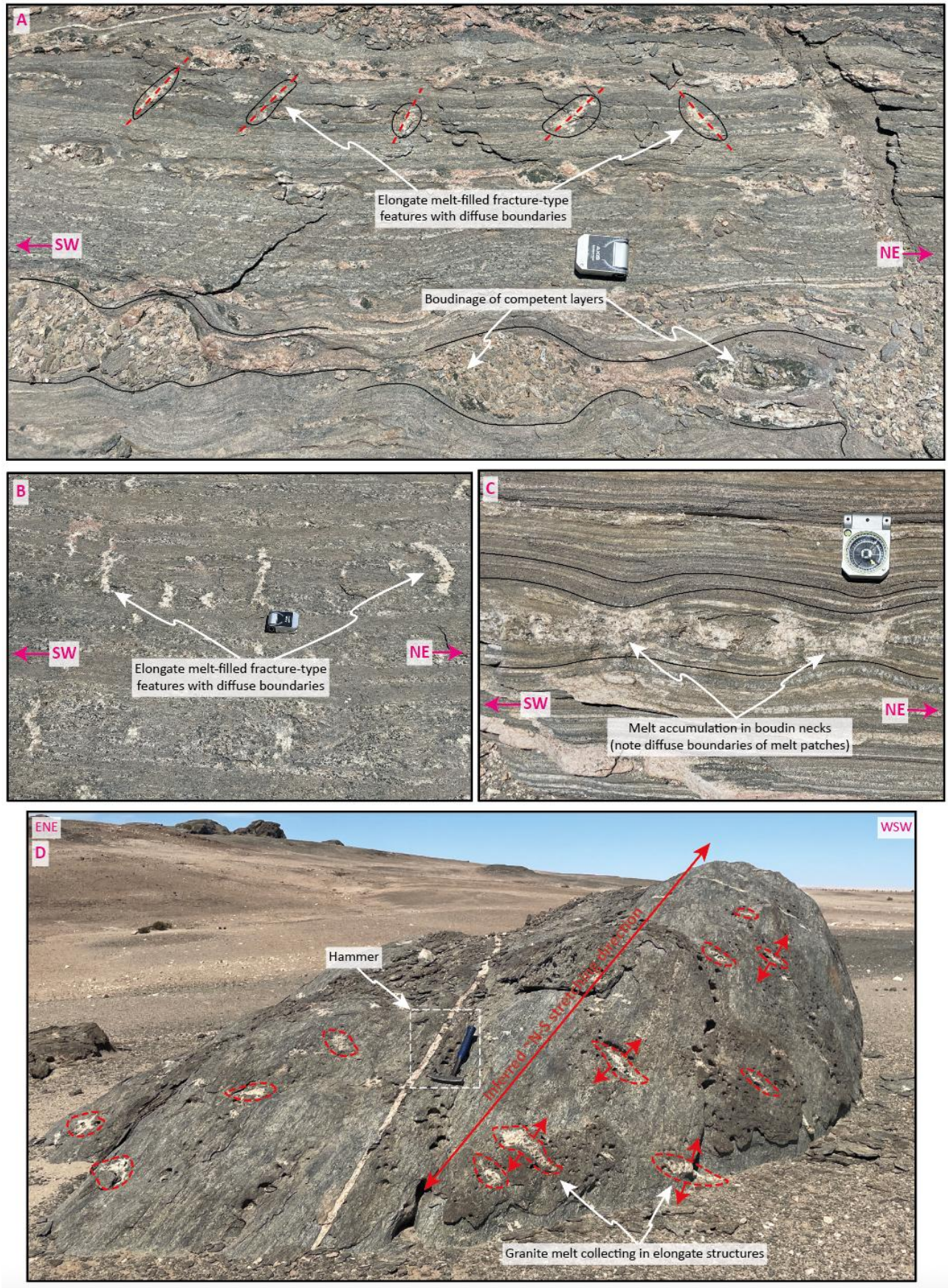

Figure 12 – Evidence for stretching associated with leucogranite migration and accumulation in dilational sites. A) Plan view outcrop showing boudinage in the bottom half of the photo. Top half reveals melt-filled fracture-type features with 2 dominant orientations which together may form a conjugate set with an acute bisector trending NW-SE. B) Plan-view outcrop with melt-filled fracture-type features trending NW-SE. C) Melt accumulation in boudin necks. D) Melt-filled fracture-type features oriented ~orthogonal to the moderately north-plunging lineation in the MS7 area.

3.5 Asymmetric sense-of-shear indicators

Sense-of-shear indicators along the Swakop River transect reveal a consistent shear sense when observed in a vertical NW–SE plane. This NW-SE plane is orthogonal to both the dominant NE–SW structural grain, and the NE–SW trending stretching, rodding, and mullion lineations. In contrast, shear-sense indicators observed in the vertical NE–SW plane — parallel to the stretching lineations — yielded ambiguous results.

Due to their inconsistency, shear-sense indicators in the NE–SW plane are not discussed further. Key examples of shear-sense indicators observed in the NW–SE plane are summarised below.

3.5.1 Top-to-SE shear in Abbabis Complex on NW-dipping limb of the Ida Dome

Strain is widely distributed throughout the stromatic migmatites, sheet-like leucogranites, and isolated rafts of metasedimentary country rock that comprise the Abbabis Complex in the core of the Ida Dome. Shallowly dipping leucogranite sheets — or melt-rich leucogranite bands where the sheets are less well developed — commonly define subtle shear zones that displace and stretch intervening rafts of relict country rock. These rafts often resemble schlieren-like structures within the migmatite complex (Figure 13). Some rafts preserve an older, steeply dipping foliation that has been visibly transposed into parallelism with the shallowly dipping leucogranite sheets along the margins of the rafts (Figure 13F). The overall geometry is comparable to S–C structures, suggesting that the leucogranite sheets and melt-rich bands acted as C-planes — small-scale shear zones that both localized strain and facilitated melt migration. These features are widespread throughout the NW-dipping limb of the Ida Dome, where they imply a consistent top-to-the-SE reverse sense of shear along shallowly NW-dipping shear bands (Figure 13).

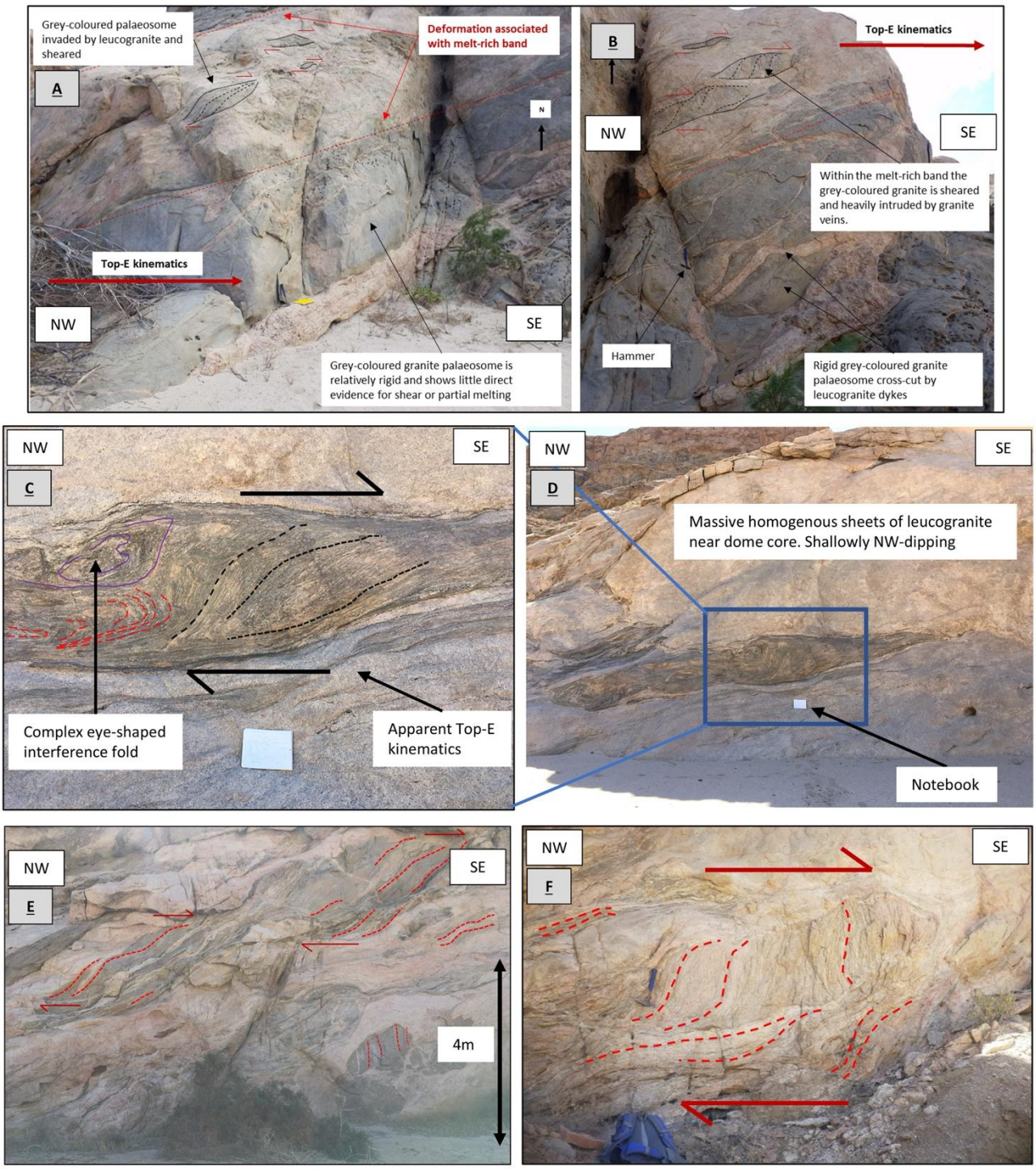

Figure 13 – Top-to-the east/SE reverse shear amongst diatexite migmatites and leucogranites of the Abbabis Complex on the NW-dipping limb of the Ida Dome. A and B) Asymmetric sense-of-shear indicators associated with a melt-rich band (with diffuse contacts between leucogranite and country rock). C and D) Schlieren-like remnant of country rock sheared between two larger NW-dipping leucogranite sheets. E) Darker-coloured country rock forms schlieren-like structures amongst leucogranite; the overall geometry resembles S-C type structures. Note how the country rock raft at the bottom right preserves a vertically-oriented foliation. F) Migmatitic country rock raft preserves a subvertical foliation but has been sheared by the melt-rich bands above and below, forming an overall S-C type geometry.

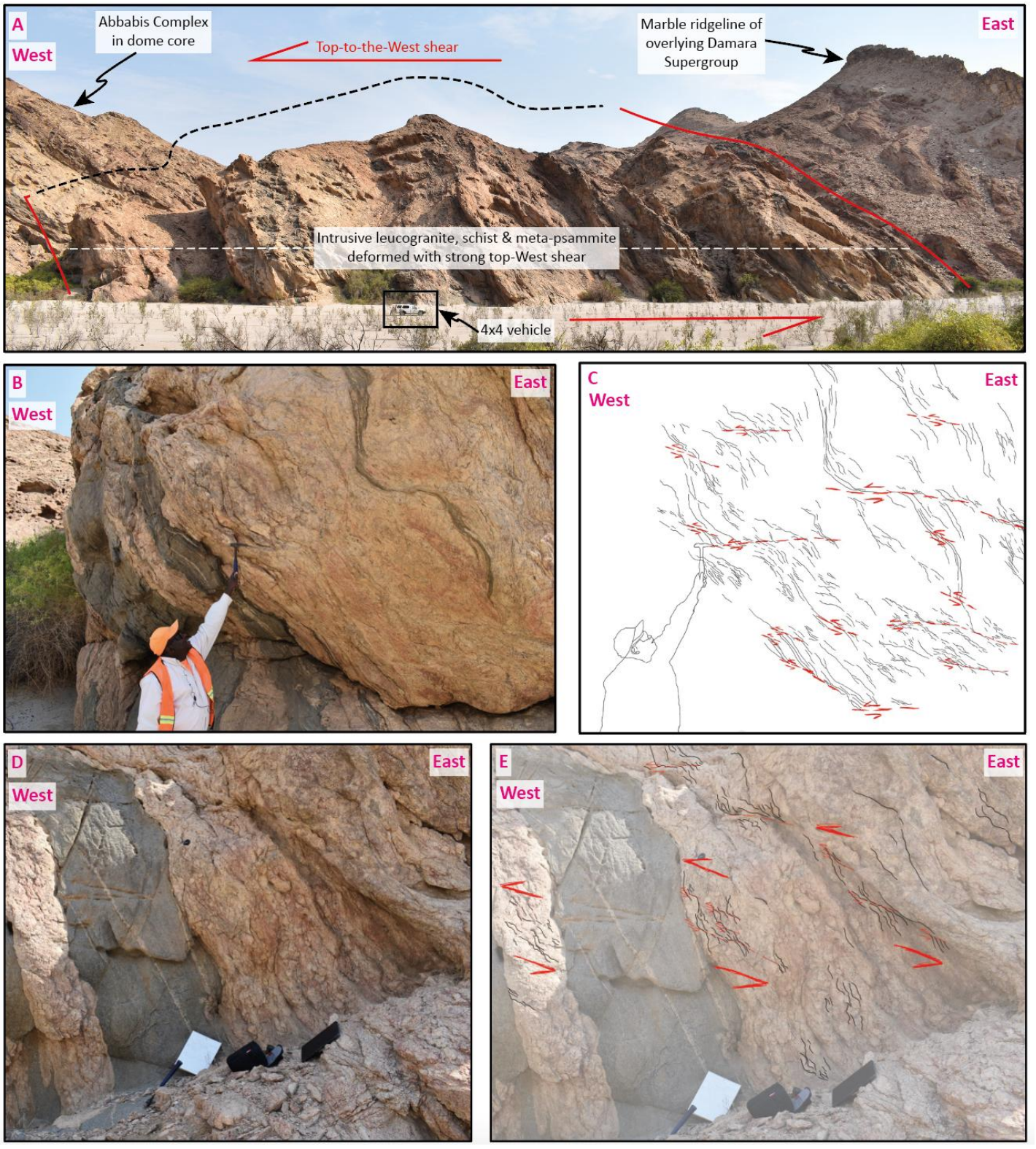

Figure 14 – Top-to-the-west reverse shear on the east-dipping limb of the Husabberg Anticlinorium. A) Far out view of the highly strained zone near the contact between the Abbabis Complex in the dome core and the overlying Damara Supergroup. B and C) Close up photo and line-drawing interpretation of S-C structures where leucogranites intruded into a schist. D and E) Nearby outcrop showing an additional close up photo and line-drawing interpretation of S-C type structures – such intense strain within the leucogranite is rare within the study area as a whole.

3.5.2 Top-to-WNW shear on ESE-dipping limb of the Husabberg Anitclinorium

A variety of rock units are intensely deformed in an ~100m thick zone at the far eastern edge of the Husabberg Anticlinorium, near to where the intrusive granites and migmatites of the Abbabis Complex in the dome core give way to more coherent overlying metasedimentary country rock units on the limb of the dome (Figure 14). S-C structures are prevalent within both quartz-biotite gneiss and metapsammitic country rocks, as well as within leucogranites that have intruded into these country rocks. The presence of such a narrow, localised, zone of intense deformation, and in particular the deformation of seemingly already crystallised leucogranite sheets, are both relatively rare observations within the study area as a whole – strain is otherwise typically pervasively distributed (as described above in the core of the Ida Dome) and leucogranites – although typically strongly folded –rarely show clear evidence for strong internal deformation in this manner. The S-C structures at this locality imply a consistent top-to-the-WNW reverse sense-of-shear along shallowly ESE-dipping C-planes (Figure 14).

3.5.3 Subtle & less obvious asymmetric fabrics

While the examples above highlight clear shear-sense indicators in the study area, these are not uniformly well developed. In many outcrops across the core of the Husabberg Anticlinorium in particular, classical S-C fabrics are absent. Nevertheless, subtle asymmetries are often preserved in the form of S- and Z-shaped foliations that resemble weakly developed or cryptic S-C structures. When viewed in a subvertical WNW–ESE plane, these patterns consistently imply reverse shear on both the WNW- and ESE-dipping limbs of the Husabberg Anticlinorium.

3.5.4 Shear associated with leucogranite dykes

Leucogranite dykes are sometimes – though not always – associated with a visible component of shear. This is indicated by deflection of the foliation on either side of the dyke (Figure 15A). When observed in the NW-SE plane along the Swakop River, this generally reveals a reverse sense-of-shear (Figure 15A). Regardless of whether a component of shear is visible or not, dykes frequently form irregular, anastomosing and interconnected networks when intruding into the Abbabis Complex and overlying Damara Supergroup along the Swakop River (Figure 15B-D). These anastomosing networks can loosely resemble conjugate sets of dykes (Figure 15B-D).

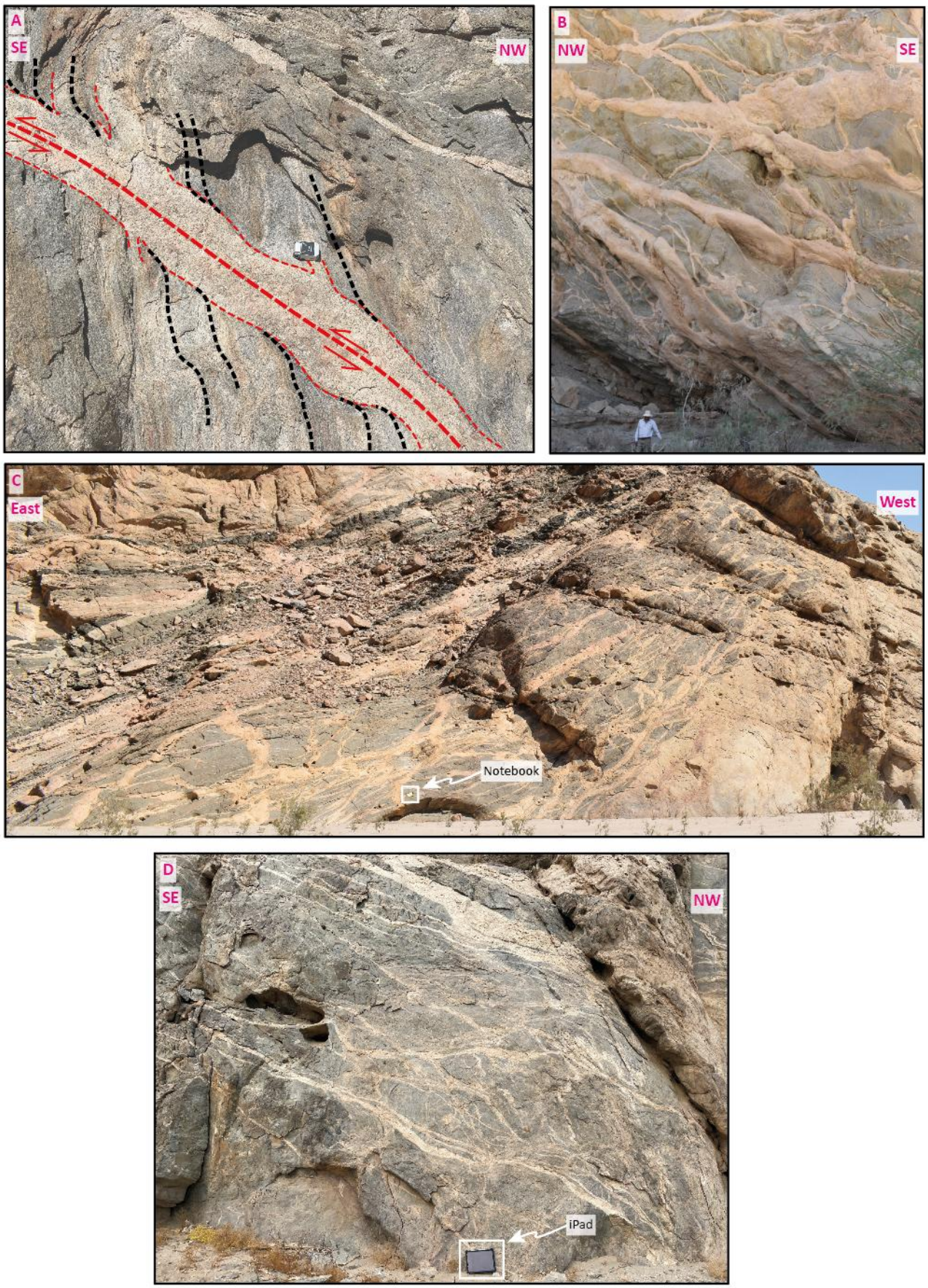

Figure 15 – Vertical outcrops showing common features of leucogranite dyke intrusion along the Swakop River. A) Dyke associated with top-to-the-SE reverse-shear amongst the Abbabis Complex in the Ida Dome. B) Anastomosing and interconnected dyke network intruding Khan Gneisses of the Damara Supergroup on the SE limb of the Ida Dome. C) Anastomosing and interconnected dyke network intruding a schist unit amongst the Abbabis Complex in the core of the Husabberg Anticlinorium. D) Anastamosing and interconnected dyke network intruding Khan Gneisses of the Damara Sueprgroup on the NW limb of the Ida Dome. Anastomosing networks can loosely resemble conjugate sets.

3.5.4 Synopsis of shear-sense indicators observed

Observations of shear sense indicators imply consistent top-to-the-SE reverse shear on NW-dipping limbs, mirrored by top-to-the-NW reverse shear on SE-dipping limbs. This symmetry supports an overall coaxial strain pattern, lacking a dominant vergence direction toward either the NW or SE. This is consistent with the upright geometry of kilometre-scale folds described above, which similarly have no consistent vergence direction (Figures 5 and 11).

4) Discussion Part I: Dyke orientation is structurally controlled by folding

4.1 Syn-tectonic leucogranite & pegmatite magmatism

Field relationships show that leucogranite magmatism occurred at the same time as both ongoing NW-SE directed shortening and simultaneous NE-SW directed stretching.

4.1.1 Leucogranite magmatism coeval with NW-SE shortening:

1. Fold structures in both the leucogranite dykes and the metamorphic country rocks are nearly identical in style and orientation (Figure 5 and Figure 11). This implies that both the leucogranites and country rocks were deformed together under the same regional stress conditions. Across all observed scales — from centimetres, metres, tens of metres, hundreds of metres, to kilometres — leucogranite intrusions are folded about predominantly shallow NE–SW plunging fold axes (Figures 7 to 11).
2. Folded leucogranite dykes cross-cut earlier - yet nearly identical - NE-SW trending fold structures in the metamorphic country rocks (e.g. Figure 8). This implies that fold structures in the country rocks were already forming at the time that leucogranites cut across them.
3. Leucogranite dykes are overwhelmingly and near-universally folded (Figures 7 to 10). NW-SE shortening may therefore have continued after the magmatic event, but magmatism did not post-date deformation.

4.1.2 Leucogranite magmatism coeval with NE-SW stretching:

A component of NE-SW stretching also occurred at the same time as leucogranite magmatism. This is indicated by the presence of leucocratic material in boudin necks trending NE-SW (Figure 12C) – parallel to the trend of both reginal km-scale fold axes and the regional stretching/rodding/mullion lineations (Figure 5). Furthermore, the presence of leucocratic material within systematic sets of ductile fracture-like features striking NW-SE (approximately at right angles to the dominant NE-SW trending stretching/rodding/mullion lineation) (Figure 12) also appears consistent with a component of NE-SW dilation.

4.1.3 Absolute age of ongoing NW-SE shortening and coeval NE-SW stretching

The field relationships summarised above show that leucogranite and pegmatite magmatism was contemporaneous with both ongoing NW-SE directed shortening and coeval NE-SW orogen-parallel stretching. Peak leucogranite magmatism in the southern Central Zone of the Damara Orogen is dated at c. 510 Ma (Jung et al., 2001; Jung and Mezger, 2003; Longridge et al., 2011; Paul et al., 2014; Jung et al., 2014; Longridge et al., 2017; Jung et al., 2017). These ages provide an absolute age constraint on the timing of ongoing deformation. We attribute this deformation to ongoing collision between the Congo and Kalahari cratons.

4.2 Folding controls dyke orientation today

Data collected in this study shows that the orientation of intrusive leucogranite dykes is consistently and systematically related to the orientation of fold structures in the country rocks. This is shown schematically in Figure 16. This relationship is consistent throughout the study area:

- Fold structures in the country rocks have upright axial planes at the regional scale (Figure 5). Leucogranite dykes are consistently folded about these same axial planes at the regional scale (Figure 11), although fold axial planes in individual outcrops locally dip at a variety of angles due to constrictional strain accumulation (Figures 7 to 9). In the 3rd dimension, folds in the dykes – like those in the metamorphic country rocks – are shallowly doubly plunging to both the NE and SW (Figure 11).
- Leucogranites retain their parallelism to map-scale fold axes even where these fold axes locally diverge from the regional NE-SW structural grain e.g. at the MS7 area (compare country-rock data in Figure 5C to leucogranite data in Figure 11C).
- Stretching and mullion lineations at individual outcrops consistently constrain the orientation of map-scale fold axes (see data in Figure 5).
    - > Consequently, outcrop-scale fold axes, stretching lineations, and mullion lineations represent mappable and measurable features which consistently and accurately constrain the orientation of folded leucogranite dykes around dome structures at larger scales.

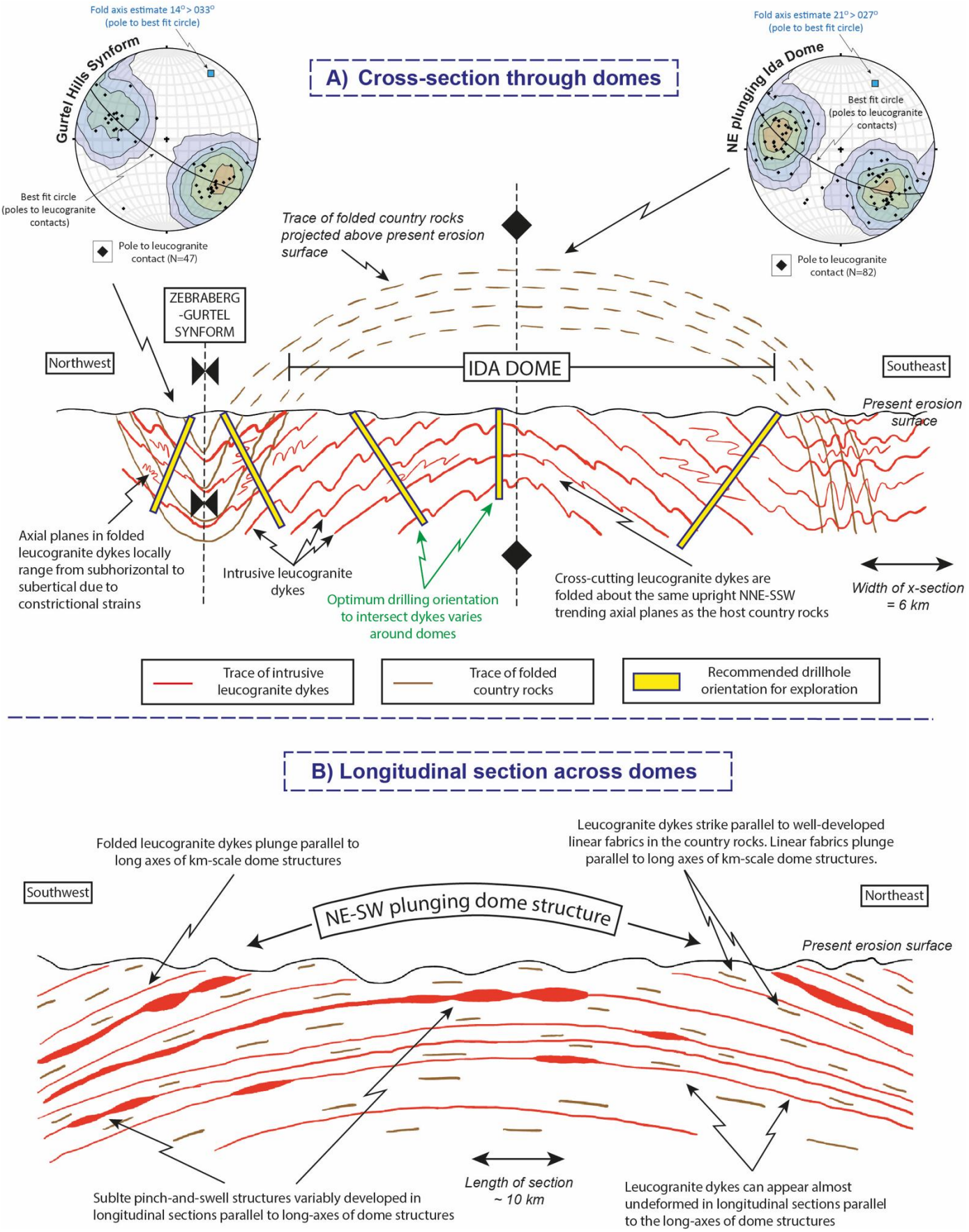

Figure 16 – Schematic illustrations showing how folded leucogranite and pegmatite dykes are systematically related to the orientation of km-scale fold structures. A) Cross-section view, and B) longitudinal section view. Recommended exploration drillhole orientation is annotated in A.

4.3 Practical applications for mineral exploration & mining

Recognition that dyke orientation is consistently and systematically linked to the geometry of km-scale dome structures (Figure 16) has important applications in the mining and mineral exploration industry. Practical applications include:

4.3.1 Better drill targeting

In areas of poor surface exposure, subsurface dyke orientation can be predicted based on known dome geometry. Dykes strike consistently parallel to stretching, rodding and mullion lineations at the outcrop-scale, and parallel to km-scale fold axes at the map scale (compare country rock data in Figure 5 to leucogranite data in Figure 11). Dyke dip angle is locally variable due to constrictional strains (Figures 7 to 9), but consistently mimics the limbs of km-scale dome structures at the map scale (Figure 11). This understanding allows more accurate planning of drill hole orientation to intersect dykes at optimal angles (ideally perpendicular to dyke planes; shown schematically in Figure 16). Benefits include (1) reducing missed targets, and (2) more accurate measurement of the thickness, grade and geometry of mineralisation to ensure tighter mineral resource estimates.

4.3.2 Predictive 3D modelling of dyke continuity

Recognition that dyke orientation is systematically related to fold structures (Figure 16) also allows dyke wireframes to be constrained to dome-controlled orientations. Lineation data, fold axes, and dome margins can be used as structural surfaces to guide interpolation, ensuring that mineralised zones are accurately placed in 3D space with respect to real-world structural architecture. This makes mineral resource models more geologically realistic, reduces uncertainty in tonnage and grade distribution, and improves reconciliation (the difference between predicted and actual ore mined). There is also potential to more easily expand known resources based on the predictable nature of dyke geometry.

4.3.3 Structural context for drill core interpretation

Oriented core logging, together with digital methods such as down-hole optical televiewer data, allow for measurements of subsurface planar and linear features such as dyke margins, foliation planes, and lineation data. This study provides the framework to show how these features can be related directly to the 3-dimensional orientation of leucogranite and pegmatite dykes (Figure 16), thereby guiding future exploration and drilling activities.

4.3.4 Refinement and future applications

We anticipate that the structural framework presented here (Figure 16) will develop further as additional data is collected by exploration and mining professionals, as well as academic researchers. Additional hypotheses which could be explored for further research include:

- Dyke orientation vs mineralisation – Leucogranite dykes are a near-ubiquitous occurrence in this area of the southern Central Zone, but few of these contain economic uranium mineralisation. The presence of mineralisation has previously been strongly correlated with a redox boundary at the contact with carbonate units (Kinnaird and Nex, 2007), but favourable structural architecture may also play a role. For example, significant uranium is often found hosted in irregularly-shaped quartz "pseudoveins" within the dykes – these can resemble unidirectional solidification textures, but they might also record migration pathways for late-stage mineralising fluids through partly-solidified crystal mush dykes (Carter et al., 2021). In the latter case, steeply orientated dykes on the limbs of km-scale domes could facilitate the buoyancy-driven upward migration of these mineralising fluids under gravity, while more shallowly-dipping dykes may hinder buoyancy-driven migration. Future studies could investigate whether steeply-dipping dykes at specific points on dome limbs have a greater uranium endowment compared to their flat-lying counterparts. Similarly, structural data on dyke orientation could be cross-referenced with other datasets such as geochemical surveys and alteration haloes. The idea that mineralising fluids may migrate semi-independently through a host, partly-crystallised, magma mush (Carter et al., 2021) has significant potential for the formulation of new ideas on the evolution of the uranium mineral system in this area. Uranium-mineralised leucogranite dykes typically cannot be separated from the regionally-widespread barren dykes on the basis of relative age or cross-cutting relationships, therefore economic mineralisation could feasibly depend on the later migration of mineralising fluids through the host magma.
- Machine learning – If the volume of structural data becomes more substantial, machine learning algorithms could potentially identify subtle or complex connections between different datasets. This might involve determining which factors (such as dyke dip, proximity to fold hinges, and alteration indices) most strongly influence mineralisation. This could be used to guide exploration strategy and identify anomalies with high potential for economic mineralisation.

4.4 Contextual background: theoretical considerations on dyke initiation and propagation

This section reviews the theoretical mechanics of dyke initiation and propagation for context only. It is useful to consider how the structural relationships observed in the field fit with current mechanical understanding of dyke emplacement under high-temperature, ductile, mid-crustal conditions. However, it is beyond the scope of this study to test each these models. This section is included solely as a basis for future research hypotheses.

4.4.1 Brittle-elastic dykes in the upper crust strike perpendicular to Sigma-3

In the brittle upper crust, dykes propagate as brittle-elastic fractures (Lister and Kerr, 1991). When stress is applied, rocks accumulate elastic strain energy up to the limit of their brittle strength (termed the fracture toughness). Once the stress intensity at the crack tip exceeds the fracture toughness, the stored elastic strain energy is released and is used to break the bonds in the rock ahead of it. This allows the fracture to grow.

In dykes, the driving stress is generated by fluid pressure of the magma (termed hydrofracturing). When magma overpressure at the crack tip creates a stress intensity exceeding the fracture toughness, the dyke propagates. The dyke propagates normal to the minimum compressive stress (sigma-3), since this is the direction of least resistance for extension (Figure 17A).

4.4.2 Ductile creep inhibits brittle-elastic dyking in the mid-crust

Under granulite-facies metamorphic conditions in the mid-crust of orogenic belts, higher temperatures allow rocks to deform continuously by ductile creep (dislocation creep, diffusion creep, and grain boundary sliding – particularly in the presence of melt). Ductile creep continuously relaxes stresses at the crack tip, preventing rocks from easily accumulating elastic strain energy. This makes it difficult for stress concentrations at the crack tip to exceed the fracture toughness, meaning that the formation of brittle-elastic dykes in high-temperature mid-crustal settings is inhibited. Overcoming the fracture toughness would require the magma pressure to build at a faster rate than the rate at which stresses are relaxed at the crack tip.

In practice, overcoming the fracture toughness in mid-crustal settings is very difficult. Firstly, Rubin (1998) showed that the critical crack length required before a hydrofracture can propagate is too long for these features to form spontaneously in a matrix containing pervasively distributed melt. Secondly, since granite melt is more viscous than basalt melt, and the compaction length in supra-solidus crust is on the order of metres to decametres (Petford, 1995; Weinberg, 1999), the rate of porous flow into a potential hydrofracture is much slower, and may be too slow to effectively drain

melt from suprasolidus crust unless the melt was already segregated into networks of melt-filled veins (Brown, 2013).

4.4.3 Mode-II ductile fracture dykes as an alternative to brittle-elastic dyking

Ductile fracturing has been proposed as an alternative mechanism for dyke initiation in high-temperature ductile environments (Figure 17B), where the formation of brittle-elastic dykes is inhibited. Rock mechanics and metallurgy studies suggest that as temperature increases, the failure mechanism transitions from brittle to conjugate ductile (Mode-II) shear failure (Gandhi and Ashby, 1979). Ductile fracturing occurs during rock creep when microscale voids grow and eventually interconnect, leading to failure – typically in the form of conjugate shear bands (Thomason, 1989). Weinberg and Regenauer-Lieb (2010) suggest that these microvoids may be filled with melt, leading to conjugate ductile fractures which act as magma channels. Once ductile fracture dykes reach a critical length, the volume of magma accumulated may be sufficient that the overpressure exceeds the fracture toughness at the crack tip, allowing ductile fracture dykes to transition into brittle-elastic dykes (Weinberg and Regenauer-Lieb, 2010).

Ductile fracture dykes can be distinguished from brittle-elastic dykes by several key criteria: (1) they originate as conjugate sets with irregular orientations (rather than as a single set normal to the tensile stress axis); (2) they are associated with shear zones (although visible shearing along fracture margins may only rarely be preserved); (3) they have blunt tips (rather than the sharp tips of brittle-elastic dykes); (4) the dykes merge with each other and form interconnected, anastomosing, networks which lack cross-cutting contacts or offsets (in contrast to brittle-elastic dykes, where multiple dyke sets commonly cross-cut one another); (5) they have tortuous margins and zigzagging trends (rather than the straight margins of brittle-elastic dykes), and (6) they intrude into high-temperature surroundings (Weinberg and Regenauer-Lieb, 2010).

4.4.4 Evidence for Mode-II ductile fracture dykes in the Damara Orogen

Figure 15 shows commonly observed features of leucogranite dyke networks intruding into both the Abbabis Complex and the Damara Supergroup along the Swakop River. These dykes bear close visual resemblance to the ductile fracture dykes envisaged by Weinberg and Regenauer-Lieb (2010), in that they are locally associated with a shear component (Figure 15A), they have geometries which roughly resemble conjugate sets (Figure 15B to 15D), they form interconnected and anastomosing networks which merge seamlessly with each other and lack cross-cutting contacts (Figure 15B to 15D), and they intruded into high-temperature granulite-facies surroundings.

However, dyke orientation is not explained by ductile fracturing alone. Conjugate sets of Mode-II ductile (shear) fractures form at oblique angles, with an acute bisector oriented parallel to

σ1, and an obtuse bisector parallel to σ 3. In the present study area, a subhorizontal NW-SE orientation of σ1 is inferred from predominantly upright NE-SW trending fold structures (Figure 5 and 11). Meanwhile, a subhorizontal NE-SW σ3 is inferred from the orientation of boudinage structures (Figure 12) and subhorizontal NE-SW trending linear fabrics (Figure 5). σ2 is by deduction oriented vertically. According to this stress configuration, the acute bisector of conjugate shear fractures should trend NW-SE, with the dykes striking at an acute angle to this (Figure 17B). In reality, leucogranite dykes throughout the study area strike dominantly NE-SW (Figure 11), in an orientation approximately orthogonal to the inferred σ1 and parallel to the inferred σ3. This mismatch represents a paradox.

4.4.5 Can folding explain the paradox of dyke orientation in the Damara Orogen?

A key observation is that leucogranite dykes are universally folded about axes that plunge shallowly NE–SW (Figure 11). These dykes may have initiated as Mode-II conjugate sets whose acute bisector was oriented NW–SE (parallel to σ_1) — this is supported by observations of melt-filled fracture-type features at high angles to the stretching direction (Figure 12), locally preserving conjugate geometries (Figure 12A). Because these ductile-fracture dykes formed at low angles to the NW–SE σ_1, they would be progressively folded and transposed about shallow NE–SW axes soon after formation, rotating toward NE–SW strikes (Figure 17C).

If emplacement occurred by ductile fracturing, as suggested by the morphological criteria above (Figure 15), then the rate of dyke propagation would be similar in order of magnitude to the ductile strain rate in the host (ductile fractures advance by creep-assisted opening of melt-filled voids, even if final rupture/linkage may transiently outpace background creep: Weinberg & Regenauer-Lieb, 2010). Consequently, formation and reorientation would be near-synchronic: NW–SE-oriented, low-angle-to-σ_1 dykes would be rotated into NE–SW at a rate comparable to their propagation, plausibly erasing their initial oblique orientations and explaining why dykes today strike consistently NE-SW (Figure 17C). We propose this as a hypothesis that needs further investigation.

4.4.6 Scope for further research

The folding model (Figure 17C) plausibly explains how dykes obtained their present-day orientation (see data in Figure 11; shown schematically in Figure 16). However, mechanical considerations on how dykes initiated and propagated are not fully resolved. For example, dykes may initiate at different orientations if principal stress axes are locally rotated around dome limbs. For previous work on dyke intrusion mechanisms in the Damara Orogen, see also Kisters et al. (2009), Hall and Kisters (2012, 2016a, 2016b), and Kruger and Kisters (2016). Further investigation of dyke initiation and propagation mechanisms are beyond the scope of this study.

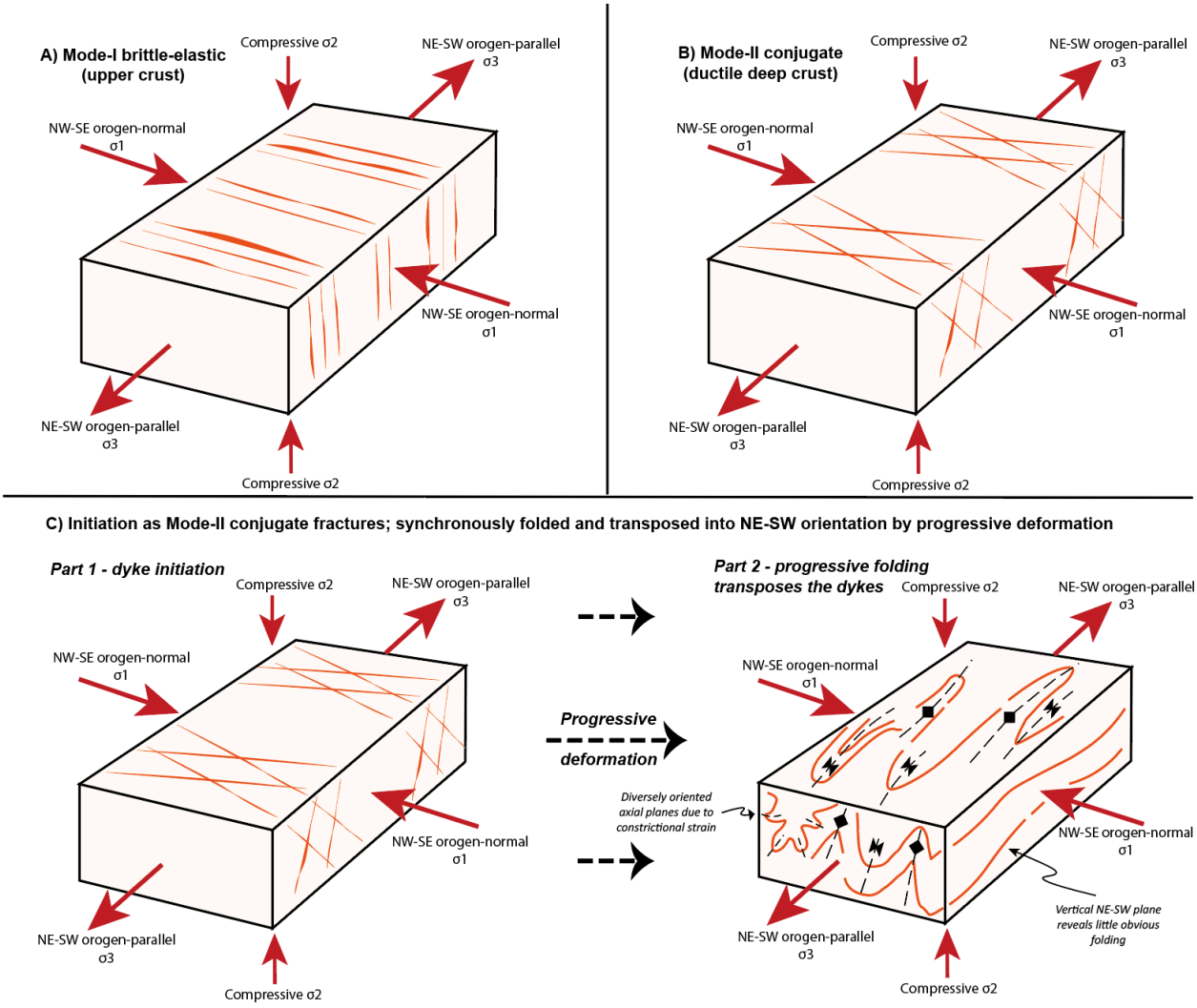

Figure 17 – Schematic illustration of different dyke intrusion mechanisms and their expected orientations relative to the regional principal stress axes inferred within the study area. A) Brittle-elastic dykes forming a single set oriented normal to the σ3 axis. B) Mode-II ductile fractures forming steeply-dipping conjugate sets with an acute bisector striking NW-SE. C) Possible explanation for observed field relationships: dykes initiate as Mode-II ductile fractures and are progressively transposed into their NE-SW striking orientations by near-synchronous deformation.

5) Discussion Part II: Insights into the regional tectonic setting

Understanding the regional tectonic setting provides critical context for producing reliable and integrated structural models at the camp to deposit scales. Here, we review different models for the regional tectonic evolution of the southern Central Zone of the Damra Orogen. Different tectonic models proposed to explain the structural evolution of the southern Central Damara Orogen include:

i. A single phase of constrictional flow (Poli & Oliver, 2001)
ii. Diapirism (Barnes & Downing 1979; Barnes, 1981; Kroner, 1984)
iii. Polyphase deformation with distinct overprinting events (Smith, 1965; Jacob et al., 1983; Longridge et al., 2011; Ormond et al., 2024)
iv. Tip-line folds above blind thrusts (Kisters et al., 2004)
v. Extensional collapse / metamorphic core complexes (Oliver 1994, 1995)

5.1 Lateral constrictional flow

5.1.1 Synopsis of lateral constrictional flow

In hot orogenic belts (T > 700–800 °C), partial melting can cause substantial melt-driven weakening of the crust (e.g., Rosenberg & Handy, 2005). Melt-driven weakening limits strain localisation, enabling the mid-crust to flow regionally as a viscous layer. Both modelling and natural examples indicate that the style and direction of flow can vary spatially and temporally, governed by the interplay between shortening-induced thickening, gravity-driven thinning, and lateral or transverse flow (Vanderhaeghe & Teyssier, 2001; Beaumont et al., 2004; Schulmann et al., 2008; Chardon et al., 2009; Jamieson & Beaumont, 2013).

Lateral constrictional flow represents a specific subtype of three-dimensional flow, which combines orogen-normal shortening with orogen-parallel stretching (Chardon et al., 2011). When the crust is too weak and gravitationally unstable to sustain further thickening, and resistance is lower along strike, continued shortening can drive lateral ductile extrusion parallel to the orogen flanks. This maintains near-constant crustal thickness. Diagnostic features include lineations parallel to orogen flanks, regionally pervasive constrictional fabrics, high temperature metamorphic conditions with widespread partial melting, and potentially also isobaric heating paths to peak metamorphic conditions. This concept aligns closely with the progressive constrictional flow model proposed for the southern Central Zone of the Damara Orogen by Poli & Oliver (2001).

5.1.2 Lateral constrictional flow in the Damara Orogen

Lateral constrictional flow can explain all structural, lithological and metamorphic characteristics of the southern Central Zone of the Damara Orogen in a single coherent model (Figure 18).

Firstly, constrictional strains are strongly developed. This is evidenced by widespread L-tectonites and prolate strain fabrics (Figure 3), as well as diversely oriented axial planes (Figures 7 to 9) and rare examples of sheath folds (Figure 6D and 6E). The dominant NE-SW orientation of linear fabrics (Figure 5) and boudinage structures (Figures 12A and 12C) provides consistent evidence for lateral constrictional stretching parallel to the flanks of the orogen. This occurred contemporaneously with leucogranite magmatism, as indicated by the presence of leucocratic material within boudin necks (Figure 12C).

Secondly, field data provides strong evidence for NW-SE shortening across the study area. Both host country rocks and intrusive leucogranite dykes are near universally folded (Figures 6 to 10), with fold axes plunging consistently NE-SW at a shallow angle (Figures 5 and 11). Major NE-SW trending km-scale dome structures are predominantly upright (as indicated by pole-to-foliation data on stereonets; Figures 5 and 11), indicating that NW-SE shortening was coaxial in nature and originated from pure shear. This is consistent with reverse-shear on NW-dipping limbs (Figure 13) being mirrored by reverse shear on SE-dipping limbs (Figure 14). Leucogranite magmatism was contemporaneous with NW-SE shortening, as indicated by intrusive dykes cutting across fold structures (e.g. Figure 8) whilst themselves being folded about axes with the same orientation (Figures 7 to 11).

Thirdly, field observations suggest that strain was pervasively distributed throughout the study area; there is little evidence that strain was localised into distinct faults or shear zones. Migmatites and leucogranites are widespread – particularly in the cores of dome structures (Toe et al., 2013; Jones et al., 2023) - indicating that large parts of the mid-crust were partially molten during the Damara Orogeny. Evidence for melt migration along shear zones (Figure 13 and 15A), and melt accumulation in boudin necks and other deformation-driven dilational zones (Figure 12), confirms that deformation occurred at the same time as magmatism throughout the study area. Together, these findings support an interpretation that the mid-crust of the orogen may have been able to flow *en-masse* at a regional scale during the peak of high-temperature metamorphism and leucogranite magmatism during the Damara Orogeny. This is consistent with numerous field and numerical models from the literature advocating for regional-scale ductile flow of partially molten orogenic mid-crust (e.g. Chardon et al., 2011; Jamieson and Beaumont et al., 2013 and references therein).

Fourthly, it has been widely recognised that dome structures in the southern Central Zone of the Damara Orogen have a complex pattern that variably meet all of Ramsay (1962) Type-1, 2 and 3 fold interference patterns (e.g. Smith, 1965; Jacob et al., 1983; Ormond et al., 2024). Ghosh et al. (1995) demonstrated experimentally that both dome-and-basin patterns and variably oriented folds with curved hinge lines can form in response to a single progressive phase of constrictional deformation. We argue that the complex dome-and-basin and fold patterns observed in the southern Central Zone of the Damara Orogen could therefore have formed as the result of the mid-crust flowing *en-masse* during a single progressive phase of lateral constrictional flow. Modern structural geology principles emphasise that strain accumulates both progressively and heterogeneously in a deforming region (Fossen et al., 2019). In the case of the southern Central Zone, the great complexity of fold structures observed (e.g. Smith, 1965; Jacob et al., 1983; Ormond et al., 2024) can be attributed to considerable spatial and temporal heterogeneities in rock composition and volume of melt present, which would make the style of this ductile flow extremely complicated at the reginal scale. Within this system, it is expected that some fold structures will locally diverge from the regional NE-SW structural grain e.g. as is observed at the MS7 fold within the present study area (Figure 5C and 11C).

Finally, we emphasise the growing body of metamorphic evidence which indicates that the heating path to peak granulite-facies regional metamorphic conditions in the southern Central Zone was isobaric – i.e. it was not associated with any significant change in pressure (Longridge et al., 2017; Jung et al., 2019; MacRoberts et al., 2025). This means that neither significant crustal thickening (e.g. due to thrust stacking), nor crustal thinning (e.g. due to gravitational collapse) occurred at this time. Our preferred model of lateral constrictional flow (Figure 18) explains how orogen-normal NW-SE directed shortening, in response to Congo-Kalahari collision, was offset by orogen-parallel NE-SW stretching and lateral extrusion of material in a constrictional strain field, together maintaining a consistent crustal thickness. This explains the isobaric heating path to peak granulite-facies conditions (see data in Longridge et al., 2017; Jung et al., 2019; MacRoberts et al., 2025). It can also explain why peak metamorphic pressures recorded in the formerly partially molten southern Central Zone (4-5 kbar – Longridge et al., 2017; Jung et al., 2019) are much lower than the peak pressures recorded in the colder, more rigid bounding thrust wedges of the Northern and Southern Zones (10.5-11.5 kbar, respectively – Goscobme et al., 2017).

Lateral Constrictional Flow in the mid-crust of the Damara Orogen

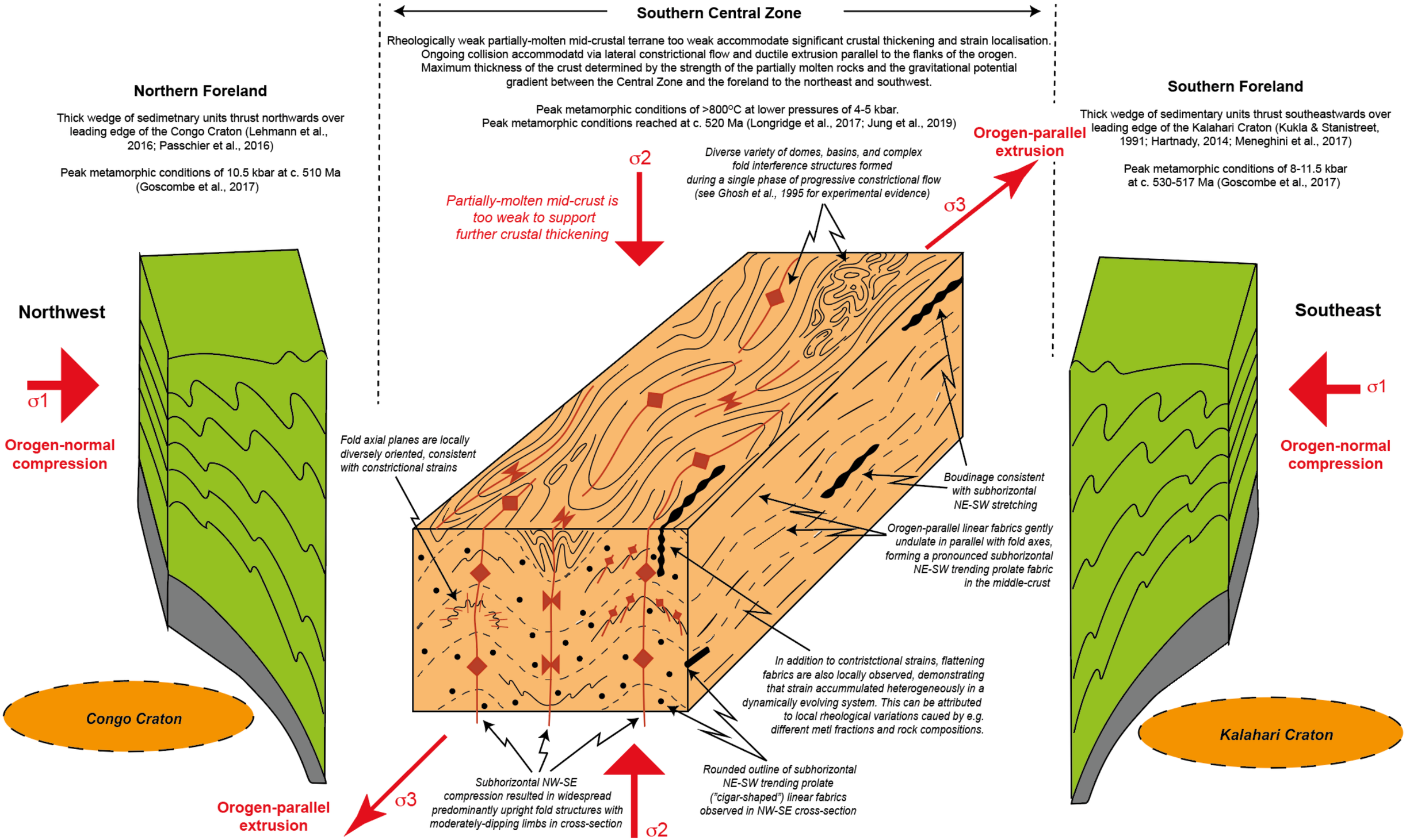

Figure 18 – Schematic illustration of lateral constrictional flow in the southern Central Zone of the Damara Orogen. The hot, partially molten and rheologyically weak southern Central Zone deformed via ductile flow on a regional scale during a single progressive phase of deformation. Since the mid-crust was too weak to support further crustal thickening, ongoing NW-SE collision was instead accommodated by NE-SW lateral extrusion of material parallel to the flanks of the orogen. The southern Central Zone is bound by thick, cold and rigid metasedimentary wedges of the Northern and Southern Zones, which were thrust onto the northern and southern forelands, respectively.

5.2 Limitations of a diapiric model

The diapiric flow model for dome formation of Eskola (1949) predicted that 1) dome formation should be synchronous with plutonic intrusion immediately beneath the dome, and 2) stretching lineations should trend radially-outwards with a top-outwards sense-of-shear.

Field evidence in this study suggests that leucogranite magmatism was indeed synchronous with dome formation (see Section 4.1). However, detailed mapping shows that stretching lineations trend consistently parallel to the long-axes of dome structures throughout the study area (overwhelmingly NE-SW); there is no evidence for any lineations trending radially outwards from the domes (Figure 5). This is consistent with the findings of Poli and Oliver (2001) further north along the Khan River. This strongly implies that the regional strain field generated by plate tectonics was more powerful than any local strain field generated by magmatically-induced buoyancy. While this does not fully rule out a component of diapiric flow contributing to dome formation, it does confirm that plate tectonic forces were the dominant driver of dome formation. This is consistent with findings from many other orogenic belts (Yin, 2004 and references therein).

5.3 *Limitations of a polyphase & overprinting deformation model*

Complexly deformed rocks that exhibit refolded folds and overprinting planar fabrics were once traditionally interpreted as the result of polyphase deformation and described in a scheme of deformation phases (D1, D2… etc). However, it is now widely recognised that regions of different structural complexity, fabrics and fabric orientations routinely arise during a single progressive deformation phase as strain accumulates heterogeneously in a deforming region. In a detailed review, Fossen et al. (2019) conclude that *"overprinting relations are known to form repeatedly during progressive deformation and are by themselves not evidence of polyphase deformation*." Fossen et al. (2019) further caution that when the concept of deformation phases is employed, the number of phases should be minimised and associated only with major tectonic events of external character, as "*uncritically defining deformation phases can easily generate a complicated discrete deformation history with no link to tectonic reality*."

In the case of the Central Zone of the Damara Orogen, problems arise with the polyphase deformation model (Smith, 1965; Jacob et al., 1983; Longridge et al., 2011; Corvino & Pretorius, 2013; Ormond et al., 2024) because the defined sequence of deformation events differs from one dome structure to another, even though these domes are often <50 km apart; this leads to great difficulty in attributing them to far-field tectonic events in the context of Congo, Kalahari and Rio de

la Plata craton collision. For example, at the Tumas Dome, Jacob et al. (1983) report that the Type-2 interference structure arose as initial WNW to NW trending folds were refolded about north-trending axes. In contrast, at the Namibfontein-Vergenoeg Dome, Ormond et al. (2024) suggest the opposite: that initial D1 fabrics were orientated north-south, before being refolded during NNW-SSE shortening (D2-D3), and finally orogen-parallel NE-SW shortening (D4). It is very difficult – and potentially impossible – to unambiguously reconcile these different sequences of deformation events within the context of a single consistent set of "*major tectonic events of external character*", as advised by Fossen et al. (2019). We propose that these complex interference patterns can be better explained by a single progressive phase of lateral constrictional flow. This model provides a simpler and more tectonically realistic interpretation, directly linked to ongoing Congo–Kalahari collision and large-scale ductile flow of a rheologically weak, partially molten mid-crustal terrane under long-lived granulite-facies conditions (Figure 18).

5.4 Limitations of a tip-line folds above blind thrusts model

Fold-and-thrust belts are best developed in the lower-grade foreland regions of orogenic belts. Here, metamorphic conditions are cooler, favouring strong strain localisation, brittle deformation, and faulting. Characteristic features of fold-and-thrust belts include displacement along low-angle thrust faults, imbricate fans, the development of thrust duplexes, and down-dip stretching lineations which record upward displacement of thrust hanging walls over the footwall. Critical wedge mechanics provides a strong theoretical basis for fold-and-thrust belt evolution in thick, layered, sedimentary basin deposits (Dahlen, 1990; Buiter, 2012). In the Damara Belt, the metasedimentary rocks on the flanks of the orogen, in the Northern and Southern zones (Figure 1), correspond well to foreland-vergent fold-and-thrust belt models. For example, in the Northern Zone, north-directed thrusting under greenschist facies conditions is represented by N-S trending stretching lineations, an axial planar cleavage, and consistent top-to-the-north foreland-vergent shear-sense indicators (Lehmann et al., 2016; Passchier et al., 2016). In the Southern Zone, the Khomas Complex and Southern Marginal Zone record consistent evidence for SE-verging folding, thrusting, and structural repetition of the sedimentary sequence, with an overall imbricate fan geometry (Miller, 1983; Kukla and Stanistreet, 1991; Hartnady, 2014; Meneghini et al., 2014, 2017; Kitt et al., 2018).

However, the southern Central Zone of the orogen does not fit fold-and-thrust belt models. Here, granulite-facies metamorphic conditions of >800^{O}C (Longridge et al., 2017; Jung et al., 2019; MacRoberts et al., 2025) are far hotter than the conditions typically associated with fold-thrust belts. These conditions were reached through an isobaric heating path (Longridge et al., 2017; Jung et al., 2019; MacRoberts et al., 2025), which rules out large-scale crustal thickening via fold-and-thrust

stacking. Rock types in the southern Central Zone consist primarily of crystalline metamorphic and magmatic rocks which lack the natural slip surfaces of thick, layered, sedimentary basin deposits. Furthermore, widespread migmatites - including the presence of melt along shear bands and in boudin necks (Figure 12C) - demonstrates that many of these rocks were partially molten at the time deformation took place. Even small volumes of melt would profoundly reduce the strength of rocks and alter their rheological behaviour (Rosenburg and Handy, 2005), limiting the ability of strain to localise into distinct shear zones and thrust faults. Perhaps most significantly, structural data from this study shows no evidence for any of the characteristic features of fold-and-thrust belts. Lineations are overwhelmingly oriented NE-SW to NNE-SSW – parallel to the flanks of the orogen (Figure 5) - rather than down-dip in a manner that could record upward displacement of thrust hanging walls towards the bounding cratons. Similarly, there is no consistent vergence direction towards either the NW or SE; structural data instead indicates that the 1st-order map-scale folds are predominantly upright structures with moderately dipping limbs verging to both the NW and SE (Figure 5). Shear-sense indicators give no consistent vergence direction; top-to-the-SE shear on NW-dipping limbs (Figure 13) is mirrored by top-to-the NW shear on SE-dipping limbs (Figure 14), implying an overall coaxial strain pattern. These features record pure shear NW-SE shortening, rather than the foreland-vergent simple-shear shortening associated with fold-and-thrust belts. Finally, distinct low-angle thrust faults are not readily observed in the field, and – due to the complexity of migmatitic rocks and various intrusive granites – unambiguous recognition of imbricate fans/thrust duplexes based on lithological mapping is not possible. We conclude that there is no meaningful evidence to support a fold-thrust belt model for the southern Central Zone.

5.5 Limitations of a metamorphic core complex associated with extensional collapse model

Oliver (1994, 1995) suggested that dome structures in the southern Central Zone of the orogen could be compared to the metamorphic core complex model of the North American cordillera. Cordilleran-style metamorphic core complexes are driven by extension of the upper crust. Extension is accommodated by hanging-wall faults above an extensional detachment. This causes thinning of the upper crust, resulting in removal of overlying weight, which in turn triggers isostatic rebound of deeper crustal rocks (Yin, 2004 and references therein). Isostatic rebound results in deep crustal rocks – often consisting of migmatites - rebounding upwards and being exposed in the cores of gneiss domes. Consequently, these migmatites often preserve metamorphic evidence for isothermal decompression from depths of >20-30 km to <10 km (Whitney et al., 2013 and references therein). Magmatism itself may either facilitate core complex formation through thermal weakening of the

crust leading to orogenic collapse, or alternatively be the result of decompression melting which arises in response to extension and upper crustal thinning (Whitney et al., 2013 and references therein).

Oliver's (1994, 1995) core complex model for the southern Central Zone of the Damara Orogen proposes that a profound ductile shear zone separates granitic gneisses in the cores of dome structures (which he interpreted as c. 1 to 2 Ga basement) from metamorphosed Neoproterozoic Damaran metasedimentary cover sequences. Different levels of the Damaran stratigraphy were proposed to have been brought down into tectonic contact with this 'basement' via extensional top-to-the-SW movement along a major detachment structure. Oliver (1995) proposed that this occurred during combined crustal NW-SE compression and SW-NE extension. This differs significantly from the classical Cordilleran metamorphic core complex model, in that Damaran extension is here suggested to be oriented orogen-parallel rather than orogen-normal.

Regardless, more recent metamorphic evidence strongly argues against a classical metamorphic core complex model for the southern Central Zone. Metamorphic data has revealed an isobaric heating path in the southern Central Zone of the orogen (Longridge et al., 2017; Jung et al., 2019; MacRoberts et al., 2025), with multiple samples from different areas recording remarkably similar granulite-facies peak metamorphic conditions of ~5 kbar and ~800 ^{O}C (Jung et al., 2019). Most importantly, neither Longridge et al. (2017) nor MacRoberts et al. (2025) recorded any evidence for decompression. Jung et al. (2019) report only *post-peak* moderate decompression followed by significant near-isobaric cooling. All data from these recent studies indicates that the peak of high-temperature metamorphism and magmatism occurred without any significant decompression; this seemingly rules out an extension-driven metamorphic core complex model for dome formation, as extension would thin the crust and cause notable decompression of migmatites and gneisses in the dome cores.

Furthermore, our detailed structural mapping identifies a similar strain pattern in both the Damaran metasedimentary units on the limbs of domes, as well as in the migmatites and gneisses in the cores of domes. This pattern consists of shallowly plunging, predominantly upright, NE-SW to NNE-SSW trending fold structures in both the host country rocks (Figure 5) and intrusive leucogranite dykes (Figure 11); these features are attributed to ongoing NW-SE directed compression during the Damara Orogeny. We could not independently verify the existence of a tectonic break or anomalously high-strain zone at the contact between the Abbabis Complex and overlying Damara Supergroup. In contrast to Oliver (1994, 1995), we found that L-tectonites are strongly developed both proximal and distal to this contact and are not themselves evidence of a relatively higher strain zone. Furthermore, no consistent asymmetric shear-sense evidence was observed to indicate that the overlying Damara metasediments had been consistently brought downwards into contact with the underlying gneisses along an extensional detachment shear zone. Overall, we consider that more

recent field and metamorphic data is inconsistent with the extensional detachment shear zone model of Oliver (1994, 1995).

Table 1 – Comparison of tectonic models presented to explain the structural evolution of the southern central Damara Orogen

Model	Evidence for	Evidence Against	Result
Polyphase deformation	✓ Ramsay Type-1, 2 and 3 fold interference structures are widely observed	× The sequence of deformation events defined differs significantly from one dome to another; this cannot be explained in the context of far-field tectonic events	×
Diapirism	✓ Widespread leucogranite magmatism occurred at the same time as dome formation	× No lineations plunge radially outwards from dome cores; they instead plunge universally parallel to regional fold axes, suggesting plate tectonic forces dominated over diapiric forces.	×
Tip-line folds above blind thrusts	✓ Widespread NE-SW trending fold axes are consistent with a strong component of NW-SE compression	× Lineations consistently trend orogen-parallel rather than down-dip, recording no evidence for foreland-vergent transport towards the bounding cratons × Regional strain pattern is coaxial and does not record evidence of foreland-vergent thrusting associated with simple shear × No distinct thrust faults observed in the study area × Isobaric heating path to peak metamorphic conditions rules out significant crustal thickening associated with thrust stacking × Granulite-facies temperatures & widespread partial melting would restrict the localisation of strain into distinct thrusts	×
Core complex / extensional collapse	✓ Migmatite-cored domes mantled by metasedimentary units superficially resemble metamorphic core complexes formed via extensional collapse	× Isobaric heating path to peak metamorphic conditions records no evidence for significant decompression, ruling out extensional tectonics associated with crustal thinning × Existence of a higher-strain zone at the Damara Supergroup – Abbabis Complex contact is not obviously supported by any field evidence collected in the present study	×
Lateral constrictional flow	✓ Prolate strain fabrics and widespread L>S tectonites provide strong evidence for regional constrictional strains ✓ Sub-horizontal NE-SW lineations and boudinage support orogen-parallel extrusion of material ✓ Pure shear NW-SE shortening is revealed by a coaxial strain pattern consisting of upright NE-SW trending fold structures ✓ Constrictional strain field (NW-SE shortening offset by NE-SW stretching) explains the isobaric heating path to peak granulite-facies conditions. ✓ Strain is pervasively distributed with little localisation into distinct shear zones – compatible with regional-scale ductile flow of the partially molten orogenic mid-crust. ✓ Favourable tectonic setting with widespread granites and migmatites and long-lived granulite-facies regional metamorphism	*N/A - this model can explain all available data*	✓

6) Conclusions

1) Orientation of leucogranite and pegmatite dykes

- Leucogranite and pegmatite dykes (c. 520–510 Ma) are syn-tectonic; they were emplaced during ongoing NW–SE shortening in a constrictional strain regime which also involved coeval NE–SW orogen-parallel stretching. This is attributed to ongoing Congo-Kalahari collision.
- Folding determines present-day dyke orientation. Leucogranites are folded into parallelism with km-scale domes. Leucogranites retain parallelism to fold axes even where these fold axes locally diverge from the NE-SW structural grain due to heterogeneous strain accumulation.
- A simple field-based conceptual model links dyke orientation to folds and lineations in the host rocks. This provides a practical framework for inferring 3D dyke geometries from limited surface mapping, drill core, or geophysical data. This directly supports drill targeting and geological modelling in mineral exploration.

2) Regional tectonic setting

- Structural and metamorphic evidence supports a model of lateral constrictional flow in the mid-crust of the Damara Orogen. High-temperature granulite-facies metamorphism triggered widespread partial melting and rheological weakening. The weak crust could not support further crustal thickening in response to ongoing Congo-Kalahari collision, therefore material was instead extruded parallel to the flanks of the orogen in a NE-SW direction. This explains both the constrictional strain patterns, the isobaric heating path to peak granulite-facies conditions, and the significantly lower peak metamorphic pressures recorded in the Central Zone compared to the bounding Northern and Southern Zones.
- Alternative tectonic models are inconsistent with the data: diapirism (contradicted by lineation trends), polyphase deformation (contradicted by radically different dome-to-dome strain histories), fold–thrust tectonics (contradicted by coaxial NW–SE shortening with little strain localisation), and extensional core-complex models (contradicted by the isobaric metamorphic path).
- The Damara Orogen records large-scale ductile flow of a hot, partially molten mid-crust. It is a superbly exposed and relatively accessible natural laboratory suitable for understanding tectonic processes within hot orogenic belts; this includes mid-crustal flow which has been suggested to be occurring beneath the Tibetan plateau today (e.g. Royden et al., 1997; Beaumont et al., 2001; Godin et al., 2006; Royden et al. 2008).

Acknowledgements

Deep Yellow Limited and Reptile Mineral Resources provided a PhD research stipend and extensive logistical support during fieldwork. The DST-NRF Centre of Excellence for Integrated Mineral and Energy Resource Analysis (DST-NRF CIMERA) provided a PhD research stipend. The Society of Economic Geologists (SEG) provided a Graduate Student Fellowship and a Student Research Grant from the McKinstry Fund. Judith Kinnaird and Paul Nex provided supervision at Wits University. Colleagues at Deep Yellow Limited and Reptile Mineral Resources provided encouragement and a sounding board for ideas. Rick Allmendinger's Stereonet software was used for the preparation of stereonets. Opinions expressed and conclusions reached are solely those of the author and should not be attributed to any of the acknowledged bodies or individuals.

References

Ashworth, L., Kinnaird, J.A., Nex, P.A.M., Harris, C., Müller, A., 2020. Origin of rare- element-mineralized Damara Belt pegmatites: a geochemical and light stable isotope study. *Lithos 372–373, 105655. https://doi.org/10.1016/j.lithos.2020.105655. ISSN: 0024-4937*.

Balaram, V., Santosh, M., Satyanarayanan, M., Srinivas, N., and Gupta, H., 2024, Lithium: A review of applications, occurrence, exploration, extraction, recycling, analysis, and environmental impact. *Geoscience Frontiers, v. 15, no. 5, 101868 p. doi: 10.1016/j.gsf.2024.101868*

Barnes, J.F.H., 1981. Some aspects of the tectonic history of the Khan-Swakop region of the Damara Belt, Namibia. *Unpublished PhD thesis, University of Leeds, United Kingdom*.

Barnes, J.F.H. and Downing, K.N. 1979. Origin of domes in the central Damara belt, Namibia. *Rev. Geol. Dynam. Geogr. Phys. 21, 383-386*.

Beaumont, C., Jamieson, R.A., Nguyen, M.H., Lee, B., 2001. Himalayan tectonics explained by extrusion of a low-viscosity crustal channel coupled to focused surface denudation. *Nature 414, 738 – 742.*

Beaumont, C., Jamieson, R.A., Nguyen, M.H., Medvedev, S., 2004. Crustal channel flows: 1. Numerical models with applications to the tectonics of the Himalayan–Tibetan orogen. *Journal of Geophysical Research 109. doi:10.1029/2003JB002809*.

Brandt, R. 1987. A revised stratigraphy for the Abbabis Complex in the Abbabis Inlier, Namibia. *South African Journal of Geology. 90, 314-323*

Brown, M., 2013. Granite: From genesis to emplacement. *Bulletin of the Geological Society of America 125, 1079–1113*.

Buiter, S. J. H. 2012. A review of brittle compressional wedge models, *Tectonophysics, 530–531, 1–17*.

Carter, L. C., Williamson, B. J., Tapster, S. R., Costa, C., Grime, G. W., & Rollinson, G. K. (2021). Crystal mush dykes as conduits for mineralising fluids in the Yerington porphyry copper district, Nevada. *Communications Earth and Environment, 2(1), 59. https://doi.org/10.1038/s43247-021-00128-4*

Cerný P, Ercit TS (2005) The classification of granitic pegmatites revisited. *Canadian Mineralogist 43: 2005-2026*

Chardon, D., D. Gapais, and F. Cagnard (2009), Flow of ultra-hot orogens: A view from the Precambrian, clues for the Phanerozoic. *Tectonophysics, 477, 105–118, doi:10.1016/j.tecto.2009.03.008.*

Chardon, D., Jayananda, M., Peucat, J.J., 2011. Lateral constrictional flow of hot orogenic crust: Insights from the Neoarchean of South India, geological and geophysical implications for

orogenic plateaux. *G3 – Geochemistry, Geophysics, Geosystems 12 (Q02005), http://dx.doi.org/10.1029/2010GC003398*.

Clark, C., Fitzsimons, I.C.W., Healy, D., Harley, S.L., 2011, How does the continental crust get really hot? *Elements, 7 (4), 235-240*

Dahlen, F. A., 1990. Critical taper model of fold-and-thrust belts and accretionary wedges, *Annu. Rev. Earth Planet. Sci., 18, 55–99.*

Dill, H.G., 2015. Pegmatites and aplites: Their genetic and applied ore geology. *Ore Geol. Rev. 69, 417– 561. https://doi.org/10.1016/j.oregeorev.2015.02.022*

Eskola, P.E., 1949, The problem of mantled gneiss domes: *Geological Society of London, Quarterly Journal, v. 104, p. 461–476.*

Fossen, H., 2016. Structural Geology, second ed. Cambridge University Press, Cambridge (ISBN 978-1-107-05764-7).

Fossen, H., Cavalcante, G. C. G., Pinheiro, R. V. L., & Archanjo, C. J. (2019). Deformation—Progressive or multiphase? *Journal of Structural Geology, 125, 82–99. https://doi.org/10.1016/j.jsg.2018.05.006*

Gandhi, C., and Ashby, M.F., 1979, Fracture-mechanism maps for materials which cleave: *F.C.C., B.C.C. and H.C.P. metals and ceramics: Acta Metallurgica, v. 27, p. 1565–1602, doi: 10.1016/0001-6160(79)90042-7.*

Geological Survey of Namibia Map Sheets 2214, 2216, 2116, 2114, 2014. *Geological Survey of Namibia, Windhoek.*

Ghosh, S. K., Khan, D., & Sengupta, S. (1995). Interfering folds in constrictional deformation. *Journal of Structural Geology, 17(10), 1361–1373. https://doi.org/10.1016/0191-8141(95)00027-B*

Godin, L., Grujic, D., Law, R.D., Searle, M.P., 2006. Channel flow, ductile extrusion and exhumation in continental collision zones: an introduction. *Geol. Soc. Spec. Publ. 268, 1–23. http://dx.doi.org/10.1144/GSL.SP.2006.268.01.01.*

Goscombe, B., Foster, D. A., Gray, D., & Wade, B. 2017a. Metamorphic response and crustal architecture in a classical collisional orogen: The Damara Belt, Namibia. *Gondwana Research, 52, 80– 124. https://doi.org/10.1016/j.gr.2017.07.006*

Goscombe, B., Foster, D.A., Gray, D., Wade, B., Marsellos, A., and Titus, J., 2017b. Deformation correlations, stress field switches and evolution of an orogenic intersection: The Pan-African Kaoko-Damara orogenic junction, Namibia: *Geoscience Frontiers, v. 8, p. 1187–1232*

Goodenough, K.M., Shaw, R.A., Smith, M., Estrade, G., Marqu, E., Bernard, C., Nex, P., 2019. Economic mineralization in pegmatites: comparing and contrasting NTF and LCT examples. *The Canadian Mineralogist 57, 753-755. https://doi.org/10.3749/canmin.AB00013*

Goslin, L.M., 2019. Deformation and partial melting in the Central Zone of the Damara Orogen, Namibia. *Unpublished Ph.D. thesis, University of the Witwatersrand.*

Groves DI, Santosh M, Goldfarb RJ, Zhang L (2018) Structural geometry of orogenic gold deposits: implications for exploration of world-class and giant deposits. *Geosci Front 9:1163–1177*

Grigson, J.L., Grigson, M.W., Kemp, A.I.S., Hagemann, S.G., and Sweetapple, M.T., 2025, The structural setting and controls of giant lithium pegmatite deposits in the Archean Pilbara craton, Western Australia: *Economic Geology, v. 120, https://doi.org/10.5382/econgeo.5170.*

Hall, D. and Kisters, A., 2012. The stabilization of self-organised leucogranite networks: Implications for melt segregation and far-field melt transfer in the continental crust. *Earth and Planetary Science Letters, 355-356: 1-12.*

Hall D. and Kisters A. 2016a. Episodic granite accumulation and extraction from the midcrust. *J Metamorph Geol 34:483–500. doi:10.1111/jmg.12190*

Hall D. and Kisters A. 2016b. From steep feeders to tabular plutons - Emplacement controls of syntectonic granitoid plutons in the Damara belt. Namibia *J Afr Earth Sci 113:51–64. https://doi.org/10.1016/j.jafrearsci.2015.10.005*

Hartnady, M.I.H. 2014. The structural evolution of an ancient accretionary prism in the Damara Belt, Namibia. *Unpublished MSc thesis, University of Cape Town, South Africa.*

International Energy Agency, 2024. Global Critical Minerals Outlook 2024. *https://www.iea.org/reports/global-critical-minerals-outlook-2024*

Jacob, R.E., Kröner, A. and Burger, A.J., 1978. Areal extent and first U-Pb age of the Pre-Damaran Abbabis complex in the central Damara belt of South West Africa (Namibia). *International Journal of Earth Sciences, 67, 706–718.*

Jacob, R.E., Snowden, P.A., Bunting, F.J.L., 1983. Geology and Structural development of the Tumas basement dome and its cover rocks. *In: Miller, R.McG. (Ed.), Evolution of the Damara Oroqen of South West Africa/Namibia. Geological Society of South Africa, Special Publication 11, pp. 409-421.*

Jamieson, R. A., and C. Beaumont (2013), On the origin of orogens. *Geological Society of America Bulletin. 125 (11-12), 1671–1702*

Jaupart, C., Mareschal, J.-C., Iarotsky, L., 2016. Radiogenic heat production in the continental crust. *Lithos 262, 398–427.*

Jones, T.L. 2021. Geological Mapping Report: Northern portion of EPL 3496. *Internal report produced on behalf of Deep Yellow Ltd, Australia.*

Jones, T.L., Otto, A., Becker, E., Wilde, A. (2023). Age of the Abbabis Complex, Damara Orogen, Namibia: 2 Ga basement or 550-500 Ma granite-migmatite complex? *Unpublished PhD Research, University of the Witwatersrand, South Africa*

Jung, S. & Mezger, K. (2003). Petrology of basement-dominated terranes: I. Regional metamorphic T-t path and geochronological constraints on Pan-African high-grade metamorphism (central Damara orogen, Namibia). *Chemical Geology, 198, 223-247.*

Jung, S., Hoernes, S., Mezger, K., 2001. Trace element and isotopic (Sr, Nd, Pb, O) arguments for a mid-crustal origin of Pan-African garnet-bearing S-type granites from the Damara orogen (Namibia). *Precambrian Research. 110 (1), 325–355. https://doi. org/10.1016/S0301-9268(01)00175-9.*

Jung, S., Berndt, J., Stracke, A., Hauff, F., Kastek, N., 2014. Anatexis of juvenile mafic to intermediate crust – constraints from major and trace element and Sr, Nd, Pb isotopes of diorites to granites (Damara orogen, Namibia). *South African Journal of Geology. 117, 149–171.*

Jung, S., Brandt, S., Bast, R., Scherer, E.E., Berndt, J., 2019. Metamorphic petrology of a high-T/low-P granulite terrane (Damara belt, Namibia) – constraints from pseudosection modelling and high-precision Lu-Hf garnet-whole rock dating. *Journal of Metamorphic Geology. 37 (1), 41–69. https://doi.org/10.1111/jmg.2019.37.issue- 110.1111/jmg.12448.*

Jung, S., Hauff, F., & Berndt, J. 2020a. Generation of a potassic to ultrapotassic alkaline complex in a syn-collisional setting through flat subduction: Constraints on magma sources and processes (Otjimbingwe alkaline complex, Damara orogen, Namibia). *Gondwana Research, 82, 267–287.*

Jung, S., Pfander, J.A., Hauff, F., Berndt, J., 2020b Crust-mantle interaction during syn- collisional magmatism – Evidence from the Oamikaub diorite and Neikhoes metagabbro (Damara orogen, Namibia). *Precambrian Research. 351, 105955. https://doi. org/10.1016/j.precamres.2020.105955.*

Kinnaird, J.A., Nex, P.A.M., 2007. A review of geological controls on uranium mineralisation in sheeted leucogranites within the Damara Orogen, Namibia. *Trans I.M.M. Applied Earth Sciences 116(2), 68-85.*

Kisters, A.F.M., Jordaan, L.S., Neumaier, K., 2004. Thrust-related dome structures in the Karibib district and the origin of orthogonal fabric domains in the south Central Zone of the Pan-African Damara belt, Namibia. *Precambrian Research 133, 283-303.*

Kisters, A.F.M., Ward, R.A., Anthonissen, C.J., Vietze, M.E., 2009, Melt segregation and far-field melt transfer in the mid-crust. *Journal of the Geological Society, 166 (5), 905-918*

Kitt, S., A. Kisters, I. Buick, and J. Kramers. 2018. Structural, Geochronological and P-T Constraints on Subduction-Accretion Processes in a Pan-African Accretionary Wedge—The Deep Level Southern Zone of the Damara Belt in Namibia. *Precambrian Research 310: 39–62.*

Knupp, K.P. 2019. Regional Airborne Geophysical Interpretation, Uranium Province, Western Namibia. *Internal report produced on behalf of Reptile Mineral Resources, Swakopmund, Namibia.*

Koopmans, L., Gardiner, N.J., St. Pierre, B., Palin, R.M., Musinga, R. and Robb, L.J. (2025) Structural Controls on Lithium Mineralization in Shear-Zone Hosted Granitic Pegmatites of the Zulu Pegmatite Field, Zimbabwe—Implications for Exploration. *Mineralium Deposita. https://doi.org/10.1007/s00126-025-01371-x*

Kroner, A. 1984. Dome structures and basement reactivation in the Pan-African Damara belt of Namibia. *In: KrOner, A. & Greiling R. (Eds.), Precambrian Tectonics Illustrated. E. Schweizerbart'sche Verlagsbuchhandlung, Stuttgart, 191-206.*

Kroner, A., Retief, E.A., Compston, W., Jacob, R.E., Burger, A.J., 1991. Single-grain and conventional zircon dating of remobilized basement gneisses in the central Damara belt of Namibia. *S. Afr. J. Geol. 94 (5/6), 379–387.*

Kruger, T., Kisters, A., 2016. Magma accumulation and segregation during regional-scale folding: the Holland's dome granite injection complex, Damara belt, Namibia. *Journal of Structural Geology* http://dx.doi.org/10.1016/j.jsg.2016.05.002.

Kukla P.A. and Stanistreet I.G., 1991. Record of the Damaran Khomas Hochland accretionary prism in central Namibia: Refutation of an "ensialic" origin of a Late Proterozoic orogenic belt. *Geology, 19: 473-476.*

Lehmann, J., Saalmann, K., Naydenov, K.V., Milani, L., Belyanin, G.A., Zwingmann, H., Charlesworth, G., Kinnaird, J.A., 2016. Structural and geochronological constraints on the Pan-African tectonic evolution of the northern Damara Belt, Namibia. *Tectonics 35 (1), 103–135.*

Lister, J.R., and Kerr, R.C., 1991, Fluid-mechanical models of crack propagation and their application to magma transport in dykes. *Journal of Geophysical Research, v. 96, p. 10,049–10,077, doi:10.1029/91JB00600.*

London, D. 2018. Ore-forming processes within granitic pegmatites. *Ore Geol Rev 101:349–383*

Longridge, L., 2012. Tectonothermal Evolution of the Southwestern Central Zone, Damara Belt, Namibia. *Unpublished Ph.D. thesis, University of the Witwatersrand, South Africa (522 pp.).*

Longridge, L., Gibson, R.L., Kinnaird, J.A. and Armstrong, R.A., 2011. Constraining the timing of deformation in the southwestern Central Zone of the Damara Belt, Namibia. *In: D.J.J. Van Hinsbergen, S.J.H. Buiter, T.H. Torsvik, C. Gaina and S.J. Webb (Editors), The Formation and Evolution of Africa: A Synopsis of 3.8 Ga of Earth History. Geological Society, London, Special Publications, 357, 107–135.*

Longridge, L., Gibson, R.L., Kinnaird, J.A. and Armstrong, R.A., 2017. New constraints on the age and conditions of LPHT metamorphism in the southwestern Central Zone of the Damara Belt, Namibia and implications for tectonic setting. *Lithos , 278-281, 361–382. doi: 10.1016/j.lithos.2017.02.006*

Longridge, L., Kinnaird, J.A., Gibson, R., Hawkesworth, C., Armstrong, R., 2018. Crystal recycling in the Damara Belt, Namibia, and interaction of the Congo and KalahariCratons–evidence from zircon U–Pb, Hf and O isotopes. *South African Journal of Geology. 121 (3),237–252.*

MacRoberts, R.J. 2025. Polyphase deformation during prolonged high-temperature, low-pressure metamorphism: An example from the Namibfontein-Vergenoeg migmatite domes, Central Zone, Damara Belt, Namibia. *Journal of Metamorphic Geology. 0. 1-35.*

Marlow, A.G., 1981. Remobilisation and primary uranium genesis in the Damaran Orogenic Belt, Namibia. *Unpublished PhD thesis, University of Leeds, United Kingdom.*

Meneghini, F., A. Kisters, I. Buick, and Å. Fagereng (2014), Fingerprints of late Neoproterozoic ridge subduction in the Pan–African Damara belt, Namibia, *Geology, doi:10.1130/g35932.1.*

Meneghini, F., Fagereng, A. and Kisters, A., 2017. The Matchless Amphibolite of the Damara belt, Namibia: unique preservation of a late Neoproterozoic ophiolitic suture. *Ofioliti , 42, 129–145., doi:10.4454/ofioliti.v42i2.452*

Milani, L., Kinnaird, J.A., Lehmann, J., Naydenov, K.V., Saalmann, K., Frei, D., Gerdes, A., 2015. Role of crustal contribution in the early stage of the Damara Orogen, Namibia: new constraints from combined U-Pb and Lu-Hf isotopes from the Goas Magmatic Complex. *Gondwana Research. 28, 961–986.*

Miller, R. 1983. The Pan-African Damara Orogen of South West Africa/Namibia. *Evolution of the Damara orogen of South West Africa/Namibia: Geological Society of South Africa Special Publication*, 11. 431-515

Miller, R. McG. & Grote, W. 1988. Geological Map of the Damara orogen, Namibia (scale 1:500,000). *Geological Survey of Namibia, Windhoek.*

Nabelek, P.I., 2020. Petrogenesis of leucogranites in collisional orogens. *Geol. Soc. Lond., Spec. Publ. 491 (1), 179–207.*

Oliver, G.J.H., 1994. Mid-crustal detachment and domes in the central zone of the Damara orogen Namibia. *Journal of African Earth Sciences 19, 331–344.*

Oliver, G.J. 1995. The Central zone of the Damara orogen, Namibia, as a deep metamorphic core complex. *Communications of the Geological Survey of Namibia, 10, 33-41.*

Ormond, R. J., J. Lehmann, P. Hasalová, and M. Elburg. 2024. Migmatite Dome as a Result of Multi-Fold Interference Pattern, in the Damara Belt, Namibia. *Journal of Structural Geology 180: 105059.*

Paul, A., S. Jung, R. L. Romer, A. Stracke, and F. Hauff (2014), Petrogenesis of synorogenic high-temperature leucogranites (Damara orogen, Namibia): Constraints from U–Pb monazite ages and Nd, Sr and Pb isotopes. *Gondwana Research, 25(4), 1614–1626, doi:10.1016/j.gr.2013.06.008.*

Passchier CW, Trouw R, Schmitt RS (2016) How to make a transverse triple junction—new evidence for the assemblage of Gondwana along the Kaoko-Damara belts, Namibia. *Geology 44(10):843– 846. https://doi.org/10.1130/G38015.1*

Petford, N., 1995, Segregation of tonalitic-trondhjemitic melts in the continental crust: The mantle connection: *Journal of Geophysical Research, v. 100, p. 15,735–15,743, doi:10.1029/94JB03259.*

Poli, L.C., Oliver, G.J.H., 2001. Constrictional deformation in the Central Zone of the Damara Orogen Namibia. *Journal of African Earth Sciences 33, 303–312.*

Ramsay, J. G., 1962. Interference patterns produced by the superposition of folds of similar type. *The Journal of Geology, 466–481. 27*

Rosenberg, C.L., Handy, M.R., 2005. Experimental deformation of partially melted granite revisited: implications for the continental crust. *Journal of Metamorphic Geology. 23, 19–28.*

Royden, L. H., Burchfiel, B. C., King, R. W., Chen, Z., Shen, F. & Liu, Y. 1997. Surface deformation and lower crustal flow in eastern Tibet. *Science, 276, 788-790.*

Royden, L.H., Burchfiel, B.C., van der Hilst, R.D., 2008. The geological evolution of the Tibetan Plateau. *Science 321, 1054–1058.*

Rubin, A.M., 1998, Dike ascent in partially molten rock: *Journal of Geophysical Research, v. 103, p. 20,901–20,919, doi: 10.1029/98JB01349.*

Sawyer, E.W., 1979. The geology of an area south-east of Walvis Bay: Lithology and field relationships. *Rep. geol. Surv. S.W. Afr. (unpublished).*

Schulmann, K., Martelat, J., Ulrich, S., Lexa, O., Štípská, P., and Becker, J.K., 2008, Evolution of microstructure and melt topology in partially molten granitic mylonite: Implications for rheology of felsic middle crust: *Journal of Geophysical Research, v. 113, B10406, doi:10.1029/2007JB005508.*

Schwark, L., Jung, S., Hauff, F., Garbe-Schonberg, D., Berndt, J., 2018. Generation of syntectonic calcalkaline, magnesian granites through remelting of pre-tectonic igneous sources – U-Pb zircon ages and Sr, Nd and Pb isotope data from the Donkerkoek granite (southern Damara Orogen, Namibia). *Lithos, 310-311, 314-331*

Searle, M., Cottle, J., Streule, M. and Waters, D., 2010. Crustal melt granites and migmatites along the Himalaya: melt source, segregation, transport and granite emplacement mechanisms. *Geological Society of America Special Papers, 472: 219-233*.

Simon, I., Jung, S., Romer, R.L., Garbe-Schonberg, D., Berndt, J., 2017. Geochemical and Nd-Sr-Pb isotope characteristics of synorogenic lower crust-derived granitoids (Central Damara orogen, Namibia). *Lithos 274–275, 397–411.*

Silva D, Groat L, Martins T, Linnen R. 2023. Structural controls on the origin and emplacement of Lithium-Bearing pegmatites. *Can J Mineralogy Petrol 61:1053–1062*

Smith, D.A.M., 1965. The geology of the area around the Khan and Swakop Rivers in SW Africa. *Geological Survey South Africa, Memoir 3, 1-113.*

Tack, L., Williams, I. and Bowden, P., 2002. SHRIMP constraints on early post-collisional granitoids of the Ida Dome, central Damara (Pan-African) Belt, western Namibia. *Abstracts of the 11th IAGOD Quadrennial Symposium and Geocongress, Windhoek, Namibia.*

Thomason, P.F., 1989, Ductile Fracture of Metals: *Oxford, UK, Pergamon Press, 219 p.*

Toé, W., Vanderhaeghe, O., André-Mayer, A.-S., Feybesse, J.-L., & Milési, J.-P. (2013). From migmatites to granites in the Pan-African Damara orogenic belt, Namibia. *Journal of African Earth Sciences, 85, 62–74. https://doi.org/10.1016/j.jafrearsci.2013.04.009*

Vanderhaeghe, O., and Teyssier, C., 2001, Partial melting and flow of orogens. *Tectonophysics, v, 342, p. 451–472.*

Ward R., Stevens G., Kisters A., 2008, Fluid and deformation induced partial melting and melt volumes in low-temperature granulite-facies metasediments, Damara Belt, Namibia: *Lithos , v. 105, p. 253–271, doi:10.1016/j.lithos.2008.04.001.*

Weinberg, R.F., 1999, Mesoscale pervasive melt migration: Alternative to dyking. *Lithos, v. 46, p. 393–410, doi: 10.1016/S0024-4937(98)00075-9.*

Weinberg, R.F., and Regenauer-Lieb, K., 2010, Ductile fractures and magma migration from source. *Geology, v. 38, p. 363–366, doi:10.1130/G30482.1.*

Whitney, D.L., Teyssier, C., Rey, P., Buck, W.R., 2013. Continental and oceanic core complexes. *Geol. Soc. Am. Bull. 125, 273–298.*

Yin, A., 2004. Gneiss domes and gneiss dome systems. *In: Whitney, D.L., Teyssier, C., Siddoway, C.S. (Eds.), Gneiss Domes and Orogeny, Geological Society of America Special Paper, vol. 380, pp. 1 – 14. 7466: Beijing, 185 pp.*